

Momentum subtraction and the  $R$ -ratio

J.A. Gracey,  
Theoretical Physics Division,  
Department of Mathematical Sciences,  
University of Liverpool,  
P.O. Box 147,  
Liverpool,  
L69 3BX,  
United Kingdom.

**Abstract.** We determine the  $R$ -ratio for massless quarks in several renormalization schemes to various loop orders. These are the momentum subtraction schemes of Celmaster and Gonsalves as well as the minimal momentum subtraction scheme. The dependence of the  $R$ -ratio on the schemes is analysed.

# 1 Introduction.

The electron-positron annihilation cross-section is a quantity which is of immense interest experimentally and theoretically. It provides an avenue to access the structure of hadrons via high energy particle beams. Known as the  $R$ -ratio the  $e^+e^-$  hadronic cross-section can be computed in perturbation theory. By this we mean that the corrections from Quantum Chromodynamics (QCD) to the leading order parton prediction can in principle be determined order by order in the strong coupling constant. Indeed as the parton model prediction depends on the squares of the parton charges, experimental measurements were used to confirm the fact that the partons themselves had fractional rather than integer values. With the advent of higher energy colliders the QCD corrections were necessary for making precision measurements of the value of the strong coupling constant. Over several decades the  $R$ -ratio has been computed to four loop orders. The leading correction was determined in [1, 2]. Subsequently, several groups independently calculated the two loop graphs in [3, 4, 5, 6]. While the three, [7, 8, 9], and four loop, [10, 11, 12], results took longer to determine. In summarizing the perturbative side of our  $R$ -ratio knowledge we have omitted some of the technical issues. First, the computations of [1, 2, 3, 4, 5, 6, 7, 8, 9, 10, 11, 12] were for the unrealistic case of massless quarks. In the real world quarks have a hierarchy of masses which have to be taken into account. In this respect there have been various analyses of the  $R$ -ratio where quark mass effects have been included. See, for example, [13, 14]. Another aspect of using a quantum field theory approach is that inevitably one has to include or estimate non-perturbative effects such as renormalons. Partly related to this is the estimation of the truncation errors on the series. This is important for making precision measurements. One way to quantify this is to use the last term of the perturbative expansion as a measure of the error bar. Though this would seem to be a limited use of the considerable effort put into calculating the four or higher loop corrections in the first place. Next in the early work of calculating the  $R$ -ratio it was noticed in [5, 6] that the choice of renormalization scheme used to handle the underlying divergences in the Feynman diagrams could lead to differing rates of the convergence of the series. This is not limited, of course, to the  $R$ -ratio but applies to any perturbatively computed quantity. In [6] the observation was made in respect of comparing the minimal subtraction ( $\overline{\text{MS}}$ ) scheme with the modified minimal subtraction ( $\overline{\text{MS}}$ ) scheme, [15]. However, in [5, 6] the  $R$ -ratio was calculated at two loops in the then recently developed momentum subtraction (MOM) scheme of [16, 17]. The results in that scheme were numerically similar to the  $\overline{\text{MS}}$  result to the same order in that the coefficients of the series appeared to be smaller than those for the  $\overline{\text{MS}}$  scheme. Indeed for certain values of  $N_f$ , which is the number of massless quark flavours, the MOM scheme seemed to have smaller numerical coefficients when compared to the  $\overline{\text{MS}}$  ones. As a consequence it was suggested in [5, 6] that the MOM scheme might be considered as the preferred renormalization scheme.

There are several advantages and disadvantages to using a MOM scheme for physical quantities instead of  $\overline{\text{MS}}$ . First, the  $\overline{\text{MS}}$  scheme is widely used since it is computationally easier to go to very high loop order. The nature of the scheme is such that only poles with respect to the regularization are removed from the quantity being computed. No finite parts are removed, aside from the contribution of  $\ln(4\pi e^{-\gamma})$ , where  $\gamma$  is the Euler-Mascheroni constant. This factor in essence is the quantity which differentiates between the  $\overline{\text{MS}}$  and  $\overline{\text{MS}}$  schemes. Hence, in light of the way the  $\overline{\text{MS}}$  scheme is defined one can essentially define the  $\overline{\text{MS}}$  renormalization constants at any external momentum configuration for the Green's function in question. For pragmatic reasons the canonical choice is a point at which it is straightforward to compute all the contributing Feynman integrals. This is assuming, of course, that such a momentum configuration does not introduce infrared divergences. Although the infrared rearrangement technique of [18, 19] circumvents this in situations where such a problem arises it allows one to extract the

unblemished renormalization constants. However, in this description of the  $\overline{\text{MS}}$  scheme we have implicitly referred to what could be regarded as a disadvantage of the scheme, which is that it is not physical. The  $\overline{\text{MS}}$  renormalization of, say, the strong coupling constant which is derived from one of the vertices of the QCD Lagrangian carries no information about the external momentum configuration which one could imagine would be relevant to a physical measurement of such a decay process. Such information of the underlying vertex or process itself could never be quantified in the residues of the poles of the renormalization constant since such poles are dependent on the regulator which is lifted at the end of the computation. Instead it would be included in the finite part of the renormalization constant and transmitted via the renormalization group evolution. This was the motivation behind the MOM schemes of [16, 17]. In [17] the 3-point vertices of the QCD Lagrangian were renormalized at the completely symmetric point. By this we mean the values of the squared momenta of the external legs were all equal. This is not sufficient in itself to define a MOM scheme as in this external momentum configuration the usual  $\overline{\text{MS}}$  coupling constant renormalization constant emerges in the computation. Instead the MOM schemes are defined by choosing the coupling constant renormalization constant such that at the symmetric point after renormalization there are no  $O(g^2)$  corrections where  $g$  is the coupling constant. Thus the MOM schemes are physical and carry information about the vertex at a specific momentum configuration unlike  $\overline{\text{MS}}$ . As an aside this external momentum configuration is non-exceptional and so there are no infrared issues. In introducing the MOM schemes of [16, 17] there are three different MOM schemes depending on whether it is defined relative to the triple gluon, ghost-gluon or quark-gluon vertices. They are denoted by MOMggg, MOMh and MOMq respectively. Though it is a moot point as to whether MOMh can be regarded as a truly physical scheme as it is defined with respect to a vertex which contains a fictitious field deriving from the gauge fixing condition. In [16, 17] the MOM schemes were defined for QCD fixed in a linear covariant gauge. In other gauges the MOM schemes will be different. In the context of the  $R$ -ratio of [5, 6] it was the MOMq scheme which was analysed in detail since that scheme is most closely aligned with the nature of the underlying Feynman graphs.

While the  $\overline{\text{MS}}$  evaluation of the  $R$ -ratio has progressed to four loops in recent years, [7, 8, 9, 10, 11, 12], the MOM scheme renormalization of QCD of [16, 17] has not been developed at the same rate and remained at the original two loop level until recently. In [20] the two loop extension to [17] was provided with the full analysis of all three 3-point vertices of the QCD Lagrangian at the fully symmetric point. Via the renormalization group this means that the three loop  $\beta$ -functions for each of the three MOM schemes are now known for all linear covariant gauges, [20]. For the Landau gauge, which will be the focus here for reasons which will be indicated later, this means that the three loop coefficient differs from that of the  $\overline{\text{MS}}$   $\beta$ -function. This is the first place the scheme difference of the  $\beta$ -functions becomes manifest. Now that the two loop extension of [17] is available it is possible to examine the MOMq scheme  $R$ -ratio of [6] to the next order and compare it with the  $\overline{\text{MS}}$  expression. This is the main purpose of this article. However, as an exercise in analysing a physical quantity in various physical and unphysical schemes we will include the MOMggg and MOMh schemes for completeness. This is partly for comparison even though MOMq is the natural scheme for the  $R$ -ratio. One aim is to see if the coefficients of the series in the different schemes show improved convergence and if there are any differences between physical and unphysical schemes. In the analysis we will include another scheme which is termed minimal-MOM and denoted by mMOM. It was introduced in [21] with the four loop mMOM QCD  $\beta$ -function deduced from the results of [22]. The renormalization group functions recorded in [21] were verified by explicit computations in [23]. The mMOM scheme is based on an extension of a property of the ghost-gluon vertex. Specifically in the Landau gauge this vertex does not get renormalized when one leg has a nullified momentum and leads to a non-renormalization theorem, [24]. In this sense the mMOM scheme could be regarded

as being similar to  $\overline{\text{MS}}$  in that the renormalization point is exceptional. Indeed examining the higher order mMOM  $\beta$ -function the mathematical structure involves rationals and the Riemann zeta functions like the  $\overline{\text{MS}}$  one and not the polylogarithms of the MOM schemes of [16, 17]. One reason for including the mMOM scheme in our analysis is that its four loop  $\beta$ -function is known, [21], which will allow us to compare its  $R$ -ratio with the  $\overline{\text{MS}}$  one at the same order. Moreover it will complement a similar analysis carried out in [21] for other quantities such as the Adler function. The actual evaluation of the  $R$ -ratio in all of these schemes is straightforward as it entails using the mapping of the coupling constant variable from one scheme to the other. In some sense one could regard the  $\overline{\text{MS}}$  evaluation of a quantity as the foundational or bare scheme from which the physical scheme value is deduced by parameter mapping. So if there is some overall difference between the unphysical  $\overline{\text{MS}}$  scheme value compared to a MOM one it should be quantifiable which is one of our secondary aims. Alternatively it could provide a novel way of extracting theoretical errors on the strong coupling constant. Finally, as this is an exercise in comparing the behaviour of the  $R$ -ratio in different renormalization schemes we have to compare like quantities. Therefore we do not include quark masses or non-perturbative renormalon features. The reason for the exclusion of the former is that the MOM schemes of [16, 17] were defined for massless quarks. Aside from [14] as far as we are aware there have been no attempts to define quark mass dependent MOM schemes.

The article is organized as follows. The relevant aspects of the renormalization group functions for each scheme are reviewed in section 2 where we also recall the coupling constant maps. Section 3 contains the  $R$ -ratio in each of the MOM schemes we consider and a discussion of the status of the convergence. A more detailed analysis is given in section 4 where the effects of the running coupling constant are included. Issues to do with gauges other than the Landau gauge are given there as well. Section 5 summarizes our conclusions.

## 2 Background.

We begin by recalling the various main features of the momentum subtraction based schemes we will be concentrating on. First, we note that our reference scheme is the  $\overline{\text{MS}}$  scheme which is the modified minimal subtraction scheme introduced in [15]. It is an extension of the original minimal subtraction (MS) scheme of [25] where the only divergences with respect to the regularizing parameter are absorbed by the renormalization constants at the point chosen for the subtraction. As noted in [15] the convergence of perturbative series appears to be quicker if one also includes a specific finite part in the renormalization constants. This is  $\ln(4\pi e^{-\gamma})$  and this quantity derives from the expansion of the  $d$ -dimensional factor in the measure of each loop integral corresponding to the volume of the  $d$ -dimensional unit sphere when the quantum field theory is dimensionally regularized. In including this extra finite piece the  $\overline{\text{MS}}$  scheme still remains a mass independent scheme and the coefficients in the  $\beta$ -function remain gauge parameter independent unlike a mass dependent scheme such as the MOM ones, [16, 17]. To assist with making contact with conventions used in different articles we will use the following form for the  $\overline{\text{MS}}$   $\beta$ -function. Defining the  $\beta$ -function in the generic scheme  $\mathcal{S}$  by

$$\beta^{\mathcal{S}}(a) = - \sum_{n=0}^{\infty} b_n^{\mathcal{S}} a^{n+1} \quad (2.1)$$

then the first four coefficients are, [26, 27, 28, 29, 30, 31, 32],

$$b_0^{\overline{\text{MS}}} = \frac{11}{3}C_A - \frac{4}{3}T_F N_f$$

$$\begin{aligned}
b_1^{\overline{\text{MS}}} &= \frac{34}{3}C_A^2 - 4T_F C_F N_f - \frac{20}{3}T_F N_f C_A \\
b_2^{\overline{\text{MS}}} &= \frac{2857}{54}C_A^3 + 2C_F^2 T_F N_f - \frac{205}{9}C_F C_A T_F N_f - \frac{1415}{27}C_A^2 T_F N_f \\
&\quad + \frac{44}{9}C_F T_F^2 N_f^2 + \frac{158}{27}C_A T_F^2 N_f^2 \\
b_3^{\overline{\text{MS}}} &= \left[ \frac{150653}{486} - \frac{44}{9}\zeta(3) \right] C_A^4 + \left[ -\frac{39143}{81} + \frac{136}{3}\zeta(3) \right] C_A^3 T_F N_f \\
&\quad + \left[ \frac{7073}{243} - \frac{656}{9}\zeta(3) \right] C_A^2 C_F T_F N_f + \left[ -\frac{4204}{27} + \frac{352}{9}\zeta(3) \right] C_A C_F^2 T_F N_f + 46C_F^3 T_F N_f \\
&\quad + \left[ \frac{7930}{81} + \frac{224}{9}\zeta(3) \right] C_A^2 T_F^2 N_f^2 + \left[ \frac{1352}{27} - \frac{704}{9}\zeta(3) \right] C_F^2 T_F^2 N_f^2 \\
&\quad + \left[ \frac{17152}{243} + \frac{448}{9}\zeta(3) \right] C_A C_F T_F^2 N_f^2 + \frac{424}{243}C_A T_F^3 N_f^3 + \frac{1232}{243}C_F T_F^3 N_f^3 \\
&\quad + \left[ \frac{704}{3}\zeta(3) - \frac{80}{9} \right] \frac{d_{AA}}{N_A} + \left[ \frac{512}{9} - \frac{1664}{3}\zeta(3) \right] \frac{N_f d_{FA}}{N_A} + \left[ \frac{512}{3}\zeta(3) - \frac{704}{9} \right] \frac{N_f^2 d_{FF}}{N_A} \quad (2.2)
\end{aligned}$$

where  $\zeta(z)$  is the Riemann zeta function,  $C_F$ ,  $C_A$  and  $T_F$  are the usual colour group Casimirs and  $N_A$  is the dimension of the adjoint representation of the colour group. At four loops several new rank four Casimirs arise, [31, 32], which are defined by

$$d_{R_1 R_2} = d_{R_1}^{abcd} d_{R_2}^{abcd} \quad (2.3)$$

where the completely symmetric tensor  $d_{R_i}^{abcd}$  is defined by

$$d_{R_i}^{abcd} = \frac{1}{6} \text{Tr} \left( T_{R_i}^a T_{R_i}^{(b} T_{R_i}^c T_{R_i}^{d)} \right) \quad (2.4)$$

with the group generators  $T^a$  in representation  $R_i$ . Here  $F$  and  $A$  denote the fundamental and adjoint representations. The number of quarks is  $N_f$  and throughout we assume that the quark masses are zero. This is primarily because the MOM scheme renormalizations were established in the absence of quark masses. We note that we use  $a = g^2/(16\pi^2)$  where  $g$  is the gauge field coupling constant. The strong coupling constant  $\alpha_s$  is related to  $g$  by  $\alpha_s = g^2/(4\pi)$ . We will use  $a$  throughout to be consistent with previous work upon which this article is based, [20], but it is straightforward to convert to other conventions.

The three main MOM schemes we consider here were introduced in [16, 17] and are based on the three 3-point vertices of the QCD Lagrangian when it is fixed in a linear covariant gauge. In other words the triple gluon, ghost-gluon and quark-gluon vertices which lead respectively to the MOMggg, MOMh and MOMq schemes. The definition of each scheme is in essence the same. The specific vertex is evaluated at the completely symmetric point where the value of the square of the momentum of each external leg is equal and set to  $(-\mu^2)$  where  $\mu$  is the scale introduced to ensure the coupling constant is dimensionless in  $d$ -dimensions when the theory is dimensionally regularized. Then at this particular external momentum configuration the coupling constant renormalization constant is defined by the condition that after renormalization there are no  $O(a)$  corrections, [16, 17]. In addition the wave function renormalization constants of the fields associated with each vertex are also constructed in a similar way, [16, 17]. In other words for the gluon, ghost and quark 2-point functions the wave function renormalization constants are determined by the condition that after renormalization there are no  $O(a)$  contributions. The two loop extension of [17] was carried out in [20]. One interesting property is that once the  $L$ th loop computation has been accomplished it is possible to deduce the  $(L+1)$ th loop renormalization group functions provided that the  $\overline{\text{MS}}$  renormalization group functions are available at that order. This is possible due to properties of the renormalization group equation and the fact that

one can construct the relation between the coupling constant as defined with respect to the  $\overline{\text{MS}}$  scheme and that in another scheme. Indeed this is the key to converting the  $R$ -ratio to the MOM schemes from the known  $\overline{\text{MS}}$  result of [1, 2, 3, 4, 5, 6, 7, 8, 9, 10, 11, 12]. Also the three loop MOM  $\beta$ -functions will be required for our comparative analysis later. The fourth momentum subtraction scheme we consider is mMOM, [21]. It derives from the Slavnov-Taylor identity for the ghost-gluon vertex in the Landau gauge. Specifically in that gauge the vertex undergoes no renormalization when an external leg momentum is set to zero. So the renormalization condition for the mMOM coupling constant renormalization is that the ghost-gluon *vertex* renormalization is the *same* as the  $\overline{\text{MS}}$  case. In this respect the mMOM scheme differs from the MOM ones of [16, 17] in that the subtraction point where the scheme is defined is exceptional. However, the main reason for including it in the present analysis is that the mMOM  $\beta$ -function is the only other  $\beta$ -function available at four loops, [22, 23].

Since the three loop MOM  $\beta$ -functions and coupling constant maps were constructed in earlier work we merely record both sets of results numerically for  $N_f$  flavours. Again this is partly due to space considerations but also to make contact with conventions. The full expressions were provided in the respective articles. However, for completeness here, we provide an attached data file where all the analytic expressions we have used are provided to assist an interested reader. For the MOM schemes at two loops special functions evaluated at specific arguments occur and to assist the conversion to numerical values we record the values we used were

$$\begin{aligned}\zeta(3) &= 1.20205690 \quad , \quad \zeta(5) = 1.03692776 \quad , \quad \zeta(7) = 1.00834928 \\ \psi'(\tfrac{1}{3}) &= 10.09559713 \quad , \quad \psi'''(\tfrac{1}{3}) = 488.1838167 \quad , \quad s_2(\tfrac{\pi}{2}) = 0.32225882 \\ s_2(\tfrac{\pi}{6}) &= 0.22459602 \quad , \quad s_3(\tfrac{\pi}{2}) = 0.32948320 \quad , \quad s_3(\tfrac{\pi}{6}) = 0.19259341\end{aligned}\tag{2.5}$$

where  $\psi(z)$  is the derivative of the logarithm of the Euler  $\Gamma$ -function and

$$s_n(z) = \frac{1}{\sqrt{3}} \Im \left[ \text{Li}_n \left( \frac{e^{iz}}{\sqrt{3}} \right) \right] \tag{2.6}$$

with  $\text{Li}_n(z)$  corresponding to the polylogarithm function. Equally we note that several other quantities can be expressed in terms of polylogarithms. For example,

$$\psi'(\tfrac{1}{3}) = \frac{2\pi^2}{3} + 2\sqrt{3}\text{Cl}_2\left(\frac{\pi}{3}\right) \tag{2.7}$$

where  $\text{Cl}_2(\theta)$  is the Clausen function which is related to the dilogarithm by

$$\text{Cl}_2(\theta) = \Im \left[ \text{Li}_2 \left( e^{i\theta} \right) \right] . \tag{2.8}$$

Therefore, the numerical values of the various  $\beta$ -functions are, [25, 26, 27, 28, 29, 30, 31, 16, 17, 20, 21],

$$\begin{aligned}\beta^{\overline{\text{MS}}}(a) &= [0.666667N_f - 11.000000] a^2 + [12.666667N_f - 102.000000] a^3 \\ &\quad + [-6.018518N_f^2 + 279.611111N_f - 1428.500000] a^4 \\ &\quad + [-1.499314N_f^3 - 405.089040N_f^2 + 6946.289617N_f - 29242.964136] a^5 \\ &\quad + O(a^6) \\ \beta^{\text{MOMggg}}(a) &= [0.666667N_f - 11.000000] a^2 + [12.666667N_f - 102.000000] a^3 \\ &\quad + [-2.658115N_f^3 + 67.089536N_f^2 - 0.565929N_f - 1570.984380] a^4 \\ &\quad + O(a^5)\end{aligned}$$

$$\begin{aligned}
\beta^{\text{MOMh}}(a) &= [0.666667N_f - 11.000000] a^2 + [12.666667N_f - 102.000000] a^3 \\
&\quad + [-21.502818N_f^2 + 617.647154N_f - 2813.492948] a^4 + O(a^5) \\
\beta^{\text{MOMq}}(a) &= [0.666667N_f - 11.000000] a^2 \\
&\quad + [12.666667N_f - 102.000000] a^3 \\
&\quad + [-22.587812N_f^2 + 588.654845N_f - 1843.65273] a^4 + O(a^5) \\
\beta^{\text{mMOM}}(a) &= [0.666667N_f - 11.000000] a^2 + [12.666667N_f - 102.000000] a^3 \\
&\quad + [-19.383310N_f^2 + 625.386670N_f - 3040.482287] a^4 \\
&\quad + [27.492640N_f^3 - 1625.402243N_f^2 + 24423.330550N_f \\
&\quad - 100541.058601] a^5 + O(a^6) .
\end{aligned} \tag{2.9}$$

Throughout all our numerical expressions will be for the  $SU(3)$  colour group. For the mMOM scheme we have provided the four loop term as the coupling constant map is known to the requisite order, [22, 23]. This is primarily because that scheme is defined with respect to a vertex function where there is a nullified external momentum. However, in this scheme and the other three MOM schemes we should emphasise that as they are mass dependent renormalization schemes their  $\beta$ -functions are not only scheme dependent at *two* loops but they also gauge dependent. This is evident in the expressions given in [16, 17] and implies, moreover, that the coupling constant mappings are gauge dependent. However, we have presented the expressions here in the Landau gauge. One reason for concentrating on this gauge is that in the path integral formulation of the gauge fixing procedure the limit  $\alpha \rightarrow 0$  is included in order that the gauge condition  $\partial^\mu A_\mu^a = 0$  is functionally implemented, where  $A_\mu^a$  is the gluon and  $\alpha$  is the gauge parameter of the linear covariant gauge. Ordinarily since one computes in  $\overline{\text{MS}}$  and the  $\beta$ -function is gauge parameter independent in that scheme, [25], one usually ignores this formal limit. Indeed one usually chooses an alternative gauge such as the Feynman gauge where the actual Feynman graphs are simpler and hence quicker to evaluate. For the mass dependent schemes one can no longer use this computational shortcut. Though we should note that in the Landau gauge the two loop term of each of the MOM  $\beta$ -functions precisely equate with the scheme independent term of the  $\overline{\text{MS}}$   $\beta$ -function as is numerically evident.

In recording the numerical value of the  $\overline{\text{MS}}$  scheme one can compare the values of the various corrections in different schemes. For example, considering the Yang-Mills case as a reference the three loop terms of the MOMggg and  $\overline{\text{MS}}$  schemes are of comparable size but smaller than the corresponding term in the other three schemes. Though for the mMOM and  $\overline{\text{MS}}$  four loop terms the former has a smaller value and differing sign. One basic lesson that one could learn from this is that a smaller coefficient in a scheme dependent term at a particular loop order in one scheme is not necessarily smaller in that scheme at the next loop order. These observations on the magnitude of the corrections in the terms in each of the schemes in question will be similar in the other quantities we consider here. For instance, the mappings of the coupling constants defined in the various schemes numerically are, [16, 17, 20, 21],

$$\begin{aligned}
a_{\text{MOMggg}} &= a + [-3.416806N_f + 26.492489] a^2 \\
&\quad + [7.687393N_f^2 - 202.085011N_f + 960.462717] a^3 + O(a^4) \\
a_{\text{MOMh}} &= a + [-1.111111N_f + 18.5482754] a^2 \\
&\quad + [1.2345678N_f^2 - 85.5559502N_f + 641.9400674] a^3 + O(a^4) \\
a_{\text{MOMq}} &= a + [-1.111111N_f + 16.7157746] a^2 \\
&\quad + [1.2345678N_f^2 - 83.1112168N_f + 472.1590953] a^3 + O(a^4)
\end{aligned}$$

$$\begin{aligned}
a_{\text{mMOM}} = & a + [-1.111111N_f + 14.083333] a^2 \\
& + \left[ 1.2345678N_f^2 - 72.454594N_f + 475.475031 \right] a^3 \\
& + \left[ -1.371742N_f^3 + 209.401255N_f^2 - 4109.724062N_f + 18652.393278 \right] a^4 \\
& + O(a^5)
\end{aligned} \tag{2.10}$$

where we use  $\overline{\text{MS}}$  are the reference scheme on the right hand side and omit the label as our convention. We do not include the mappings of the gauge parameter in the various schemes since we have chosen the Landau gauge. All the gauge parameter mappings from the MOM schemes to the  $\overline{\text{MS}}$  scheme are proportional to the gauge parameter. So choosing the Landau gauge in one scheme implies that one has to use the Landau gauge in the other scheme. Related to the coupling constant scheme mappings are the relations between the  $\Lambda$  parameters in the various schemes. This parameter in essence is the constant of integration when one solves the first order differential equation defining the running of the coupling constant in terms of the  $\beta$ -function. It is different in different schemes but the ratio of  $\Lambda$  in two schemes can be determined by a simple one loop calculation. As it will play a role in our analysis later we record the relations we will need for the various schemes and values of  $N_f$  in Table 1 for the Landau gauge for completeness where MOMi indicates one of the four MOM schemes of interest. Those for MOMggg, MOMh and MOMq were given in [17] and the mMOM values were provided in [21].

$N_f$	MOMggg	MOMh	MOMq	mMOM
3	2.4654	2.3286	2.1032	1.8171
4	2.1587	2.3308	2.0881	1.7831
5	1.8471	2.3335	2.0706	1.7440
6	1.5341	2.3366	2.0499	1.6985

Table 1. Values of  $\Lambda^{\text{MOMi}}/\Lambda^{\overline{\text{MS}}}$  for  $SU(3)$  in the Landau gauge.

### 3 MOM $R$ -ratios.

Having discussed the various renormalization schemes and the relation between them we can construct the expressions for the  $R$ -ratio of the MOM schemes. The starting point is the  $\overline{\text{MS}}$   $R$ -ratio, [1, 2, 3, 4, 5, 6, 7, 8, 9, 10, 11, 12]. To reproduce the two loop MOMq correction of [5, 6] the method is the same as that of the previous section for the renormalization group functions. One maps the  $\overline{\text{MS}}$  coupling constant to the coupling constant of the MOM scheme of interest. Therefore to repeat the exercise of [5, 6] to the next order we begin with the three and four loop  $\overline{\text{MS}}$   $R$ -ratios of [7, 8, 9, 10, 11, 12]. The latter is required for the conversion to the mMOM scheme since the coupling constant map is known to the right order. For reference, we note that the three loop  $R$ -ratio is

$$\begin{aligned}
R^{\overline{\text{MS}}}(s) = & N_F \sum_f Q_f^2 \left[ 1 + 3C_F a \right. \\
& + \left[ \left[ \frac{123}{2} - 44\zeta(3) \right] C_F C_A - \frac{3}{2} C_F^2 + [-22 + 16\zeta(3)] C_F T_F N_f \right] a^2 \\
& + \left[ -\frac{69}{2} C_F^3 + [-127 - 572\zeta(3) + 880\zeta(5)] C_F^2 C_A \right. \\
& \left. \left. + \left[ \frac{90445}{54} - \frac{10948}{9} \zeta(3) - \frac{440}{3} \zeta(5) \right] C_F C_A^2 \right] a^3 \right]
\end{aligned}$$

$$\begin{aligned}
& + [-29 + 304\zeta(3) - 320\zeta(5)] C_F^2 T_F N_f \\
& + \left[ -\frac{31040}{27} + \frac{7168}{9}\zeta(3) + \frac{160}{3}\zeta(5) \right] C_F C_A T_F N_f \\
& + \left[ \frac{4832}{27} - \frac{1216}{9}\zeta(3) \right] C_F T_F^2 N_f^2 - \pi^2 \left[ \frac{11}{3} C_A - \frac{4}{3} T_F N_f \right]^2 C_F \Big] a^3 \Big] \\
& + \left( \sum_f Q_f \right)^2 d^{abc} d^{abc} \left[ \frac{11}{3} - 8\zeta(3) \right] a^3 + O(a^4)
\end{aligned} \tag{3.1}$$

where  $s$  is the centre of mass energy,  $N_F$  is the dimension of the fundamental representation,  $Q_f$  is the charge of the  $N_f$  active quarks and  $d^{abc}$  is the totally symmetric rank 3 tensor. It is related to the trace of three colour group generators and originates from three loop diagrams where there are two separate quark loops. The appearance of  $\pi^2$  derives from the imaginary part of the mapping of the momentum from the Euclidean to the physical region as discussed, for instance, in [7]. The convention is that the scheme label on the quantity on the left side indicates the scheme the coupling constant is in on the right hand side. In order to save space we have not included the four loop term which is already available in [10, 11, 12].

We can now take the analytic form for the coupling constant map and convert (3.1) to each of the MOM schemes. For MOMggg we have

$$\begin{aligned}
R^{\text{MOMggg}}(s) = & N_F \sum_f Q_f^2 \Big[ 1 + 3C_F a \\
& + \left[ 16\zeta(3) - 14 - \frac{64}{27}\pi^2 + \frac{32}{9}\psi' \left( \frac{1}{3} \right) \right] N_f T_F C_F \\
& + \left[ \frac{79}{2} - 44\zeta(3) + \frac{23}{27}\pi^2 - \frac{23}{18}\psi' \left( \frac{1}{3} \right) \right] - \frac{3}{2} C_F^2 \Big] a^2 \\
& + \left[ \left[ \frac{6368}{81}\zeta(3)\pi^2 - \frac{29317}{54} + \frac{3520}{9}\zeta(3) + \frac{160}{3}\zeta(5) - \frac{2866}{81}\pi^2 \right. \right. \\
& - \frac{2560}{2187}\pi^4 - 240s_2 \left( \frac{\pi}{6} \right) + 480s_2 \left( \frac{\pi}{2} \right) + 400s_3 \left( \frac{\pi}{6} \right) - 320s_3 \left( \frac{\pi}{2} \right) \\
& + \frac{1829}{27}\psi' \left( \frac{1}{3} \right) - \frac{3184}{27}\psi' \left( \frac{1}{3} \right) \zeta(3) + \frac{5152}{729}\psi' \left( \frac{1}{3} \right) \pi^2 \\
& - \frac{1288}{243} \left( \psi' \left( \frac{1}{3} \right) \right)^2 - \frac{4}{9}\psi''' \left( \frac{1}{3} \right) - \frac{5}{9} \ln^2(3)\sqrt{3}\pi + \frac{20}{3} \ln(3)\sqrt{3}\pi \\
& \left. + \frac{145}{243}\sqrt{3}\pi^3 \right] N_f T_F C_F C_A \\
& + \left[ 14 + 256\zeta(3) - 320\zeta(5) - \frac{128}{27}\pi^2 + \frac{64}{9}\psi' \left( \frac{1}{3} \right) \right] N_f T_F C_F^2 \\
& + \left[ \frac{2252}{27} - \frac{2048}{81}\zeta(3)\pi^2 - \frac{448}{9}\zeta(3) + \frac{1520}{81}\pi^2 + \frac{7168}{2187}\pi^4 \right. \\
& - \frac{832}{27}\psi' \left( \frac{1}{3} \right) + \frac{1024}{27}\psi' \left( \frac{1}{3} \right) \zeta(3) - \frac{7168}{729}\psi' \left( \frac{1}{3} \right) \pi^2 \\
& \left. + \frac{1792}{243} \left( \psi' \left( \frac{1}{3} \right) \right)^2 \right] N_f^2 T_F^2 C_F \\
& + \left[ \frac{1397759}{1728} - \frac{2024}{81}\zeta(3)\pi^2 - \frac{90781}{144}\zeta(3) - \frac{440}{3}\zeta(5) - \frac{329}{9}\pi^2 \right. \\
& - \frac{27181}{17496}\pi^4 + 519s_2 \left( \frac{\pi}{6} \right) - 1038s_2 \left( \frac{\pi}{2} \right) - 865s_3 \left( \frac{\pi}{6} \right) \\
& \left. + 692s_3 \left( \frac{\pi}{2} \right) + \frac{104}{3}\psi' \left( \frac{1}{3} \right) + \frac{1012}{27}\psi' \left( \frac{1}{3} \right) \zeta(3) \right]
\end{aligned}$$

$$\begin{aligned}
& -\frac{3703}{2916}\psi'(\tfrac{1}{3})\pi^2 + \frac{3703}{3888}(\psi'(\tfrac{1}{3}))^2 + \frac{427}{576}\psi'''(\tfrac{1}{3}) \\
& + \frac{173}{144}\ln^2(3)\sqrt{3}\pi - \frac{173}{12}\ln(3)\sqrt{3}\pi - \frac{5017}{3888}\sqrt{3}\pi^3 \Big] C_F C_A^2 \\
& + \left[ 880\zeta(5) - 105 - 572\zeta(3) - \frac{23}{27}\pi^2 + \frac{23}{18}\psi'(\tfrac{1}{3}) \right] C_F^2 C_A \\
& - \frac{69}{2}C_F^3 \Big] a^3 \Big] + \left( \sum_f Q_f \right)^2 d^{abc}d^{abc} \left[ \frac{11}{3} - 8\zeta(3) \right] a^3 \\
& + O(a^4)
\end{aligned} \tag{3.2}$$

at three loops. For all the MOM schemes at this order the  $d^{abc}d^{abc}$  term will be formally the same as the  $\overline{\text{MS}}$  case. However, the numbers associated with the definition of the symmetric point renormalization of the underlying 3-point vertices naturally appear in the full expression. Equally for the MOMq case we have

$$\begin{aligned}
R^{\text{MOMq}(s)} = & N_F \sum_f Q_f^2 \Big[ 1 + 3C_F a \\
& + \left[ -\frac{46}{3} + 16\zeta(3) \right] N_f T_F C_F \\
& + \left[ \frac{407}{12} - 44\zeta(3) - \frac{13}{9}\pi^2 + \frac{13}{6}\psi'(\tfrac{1}{3}) \right] C_F C_A \\
& + \left[ \frac{21}{2} + \frac{8}{9}\pi^2 - \frac{4}{3}\psi'(\tfrac{1}{3}) \right] C_F^2 \Big] a^2 \\
& + \left[ -\frac{1553}{3} - \frac{416}{27}\zeta(3)\pi^2 + \frac{1004}{3}\zeta(3) + \frac{160}{3}\zeta(5) + \frac{2840}{81}\pi^2 - \frac{8}{27}\pi^4 \right. \\
& - 24s_2(\tfrac{\pi}{6}) + 48s_2(\tfrac{\pi}{2}) + 40s_3(\tfrac{\pi}{6}) - 32s_3(\tfrac{\pi}{2}) - \frac{1024}{27}\psi'(\tfrac{1}{3}) \\
& + \frac{208}{9}\psi'(\tfrac{1}{3})\zeta(3) + \frac{1}{9}\psi'''(\tfrac{1}{3}) - \frac{1}{18}\ln^2(3)\sqrt{3}\pi + \frac{2}{3}\ln(3)\sqrt{3}\pi \\
& + \left. \frac{29}{486}\sqrt{3}\pi^3 \right] N_f T_F C_F C_A \\
& + \left[ -\frac{346}{3} + \frac{256}{27}\zeta(3)\pi^2 + 384\zeta(3) - 320\zeta(5) - \frac{880}{81}\pi^2 \right. \\
& + \left. \frac{440}{27}\psi'(\tfrac{1}{3}) - \frac{128}{9}\psi'(\tfrac{1}{3})\zeta(3) \right] N_f T_F C_F^2 \\
& + \left[ 96 - 64\zeta(3) - \frac{16}{9}\pi^2 \right] N_f^2 T_F^2 C_F \\
& + \left[ \frac{7555}{12} + \frac{1144}{27}\zeta(3)\pi^2 - \frac{18535}{48}\zeta(3) - \frac{440}{3}\zeta(5) - \frac{32159}{648}\pi^2 \right. \\
& + \frac{983}{486}\pi^4 - \frac{171}{2}s_2(\tfrac{\pi}{6}) + 171s_2(\tfrac{\pi}{2}) + \frac{285}{2}s_3(\tfrac{\pi}{6}) - 114s_3(\tfrac{\pi}{2}) \\
& + \frac{23447}{432}\psi'(\tfrac{1}{3}) - \frac{572}{9}\psi'(\tfrac{1}{3})\zeta(3) - \frac{1759}{324}\psi'(\tfrac{1}{3})\pi^2 \\
& + \frac{1759}{432}(\psi'(\tfrac{1}{3}))^2 - \frac{23}{288}\psi'''(\tfrac{1}{3}) - \frac{19}{96}\ln^2(3)\sqrt{3}\pi \\
& + \left. \frac{19}{8}\ln(3)\sqrt{3}\pi + \frac{551}{2592}\sqrt{3}\pi^3 \right] C_F C_A^2 \\
& + \left[ \frac{2441}{12} - \frac{704}{27}\zeta(3)\pi^2 - 930\zeta(3) + 880\zeta(5) - \frac{2665}{81}\pi^2 - \frac{688}{243}\pi^4 \right. \\
& + \left. 252s_2(\tfrac{\pi}{6}) - 504s_2(\tfrac{\pi}{2}) - 420s_3(\tfrac{\pi}{6}) + 336s_3(\tfrac{\pi}{2}) \right]
\end{aligned}$$

$$\begin{aligned}
& + \frac{2665}{54} \psi' \left( \frac{1}{3} \right) + \frac{352}{9} \psi' \left( \frac{1}{3} \right) \zeta(3) + \frac{796}{81} \psi' \left( \frac{1}{3} \right) \pi^2 \\
& - \frac{199}{27} (\psi' \left( \frac{1}{3} \right))^2 - \frac{1}{6} \psi''' \left( \frac{1}{3} \right) + \frac{7}{12} \ln^2(3) \sqrt{3} \pi - 7 \ln(3) \sqrt{3} \pi \\
& - \frac{203}{324} \sqrt{3} \pi^3 \Big] C_F^2 C_A \\
& + \left[ \frac{33}{2} - 56 \zeta(3) + \frac{116}{3} \pi^2 - \frac{176}{243} \pi^4 + 48 s_2 \left( \frac{\pi}{6} \right) - 96 s_2 \left( \frac{\pi}{2} \right) \right. \\
& - 80 s_3 \left( \frac{\pi}{6} \right) + 64 s_3 \left( \frac{\pi}{2} \right) - 58 \psi' \left( \frac{1}{3} \right) - \frac{400}{81} \psi' \left( \frac{1}{3} \right) \pi^2 \\
& + \frac{100}{27} (\psi' \left( \frac{1}{3} \right))^2 + \frac{8}{9} \psi''' \left( \frac{1}{3} \right) + \frac{1}{9} \ln^2(3) \sqrt{3} \pi - \frac{4}{3} \ln(3) \sqrt{3} \pi \\
& \left. - \frac{29}{243} \sqrt{3} \pi^3 \right] C_F^3 \\
& - \frac{69}{2} C_F^3 \Big] a^3 \Big] + \left( \sum_f Q_f \right)^2 d^{abc} d^{abc} \left[ \frac{11}{3} - 8 \zeta(3) \right] a^3 \\
& + O(a^4) .
\end{aligned} \tag{3.3}$$

As this MOMq scheme was the scheme which Celmaster and Gonsalves used for their discussion of the magnitude of the higher order terms given the underlying quark nature of the  $R$ -ratio, we have checked that the  $O(a^2)$  term is in precise agreement with the corresponding term of [5, 6].

Rather than repeat similar expressions for the other schemes as they add no further enlightenment and are included in the associated data file anyway, we present the results in numerical form. This is more practical for relative comparison. To facillitate this we use a similar notation to [10, 11, 12] and define  $r^{\mathcal{S}}(s)$  by

$$R^{\mathcal{S}}(s) = N_F \left( \sum_f Q_f^2 \right) r^{\mathcal{S}}(s) . \tag{3.4}$$

For arbitrary  $N_f$  we have for  $SU(3)$

$$\begin{aligned}
r^{\overline{\text{MS}}}(s) &= 1 + 4.000000a + [-1.844726N_f + 31.771318] a^2 \\
&+ [-0.331415N_f^2 - 76.808579N_f - 424.763877 - 26.443505\eta^Q] a^3 \\
&+ [5.508123N_f^3 - 204.143191N_f^2 + 4806.339848N_f + 49.0568463N_f\eta^Q \\
&- 1521.214892\eta^Q - 40091.676394] a^4 + O(a^5) \\
r^{\text{MOMggg}}(s) &= 1 + 4.000000a + [11.822499N_f - 74.198637] a^2 \\
&+ [49.709397N_f^2 - 401.928165N_f - 335.201605 \\
&- 26.443505\eta^Q] a^3 + O(a^4) \\
r^{\text{MOMh}}(s) &= 1 + 4.000000a + [2.599718N_f - 42.421783] a^2 \\
&+ [0.507465N_f^2 + 74.704019N_f - 1418.822320 \\
&- 26.443505\eta^Q] a^3 + O(a^4) \\
r^{\text{MOMq}}(s) &= 1 + 4.000000a + [2.599718N_f - 35.091780] a^2 \\
&+ [0.507465N_f^2 + 90.741952N_f - 1140.227694
\end{aligned}$$

$$\begin{aligned}
& - 26.443505\eta^Q \Big] a^3 + O(a^4) \\
r^{\text{mMOM}}(s) = & 1 + 4.000000a + [2.599718N_f - 24.562015] a^2 \\
& + \left[ 0.507465N_f^2 + 85.202150N_f - 1634.833914 - 26.443505\eta^Q \right] a^3 \\
& + \left[ 3.058056N_f^3 - 230.126428N_f^2 + 4880.206236N_f - 17400.630112 \right. \\
& \left. - 39.088169N_f\eta^Q - 403.976819\eta^Q \right] a^4 + O(a^5)
\end{aligned} \tag{3.5}$$

where we have introduced

$$\eta^Q = \frac{\left( \sum_f Q_f \right)^2}{\left( \sum_f Q_f^2 \right)}. \tag{3.6}$$

In effect (3.5) represents the main results of the article. With these expressions one sees a similar feature to the  $\beta$ -functions in the sense that comparing with the  $\overline{\text{MS}}$  expression as the reference there is no clear pattern to the magnitude or signs of the coefficients. This is borne out if they are evaluated explicitly for various values of  $N_f$ . For the non-singlet (NS) case, defined by  $\eta^Q = 0$ , in ascending order of  $N_f$  we have

$$\begin{aligned}
r^{\overline{\text{MS}}}(s) \Big|_{N_f=3}^{\text{NS}} &= 1 + 4.000000a + 26.237139a^2 - 658.172348a^3 \\
& - 27361.226258a^4 + O(a^5) \\
r^{\text{MOMggg}}(s) \Big|_{N_f=3}^{\text{NS}} &= 1 + 4.000000a - 38.731139a^2 - 1039.601525a^3 + O(a^4) \\
r^{\text{MOMh}}(s) \Big|_{N_f=3}^{\text{NS}} &= 1 + 4.000000a - 34.622629a^2 - 1190.143080a^3 + O(a^4) \\
r^{\text{MOMq}}(s) \Big|_{N_f=3}^{\text{NS}} &= 1 + 4.000000a - 27.292626a^2 - 863.434654a^3 + O(a^4) \\
r^{\text{mMOM}}(s) \Big|_{N_f=3}^{\text{NS}} &= 1 + 4.000000a - 16.762861a^2 - 1374.660279a^3 \\
& - 4748.581755a^4 + O(a^5)
\end{aligned} \tag{3.7}$$

$$\begin{aligned}
r^{\overline{\text{MS}}}(s) \Big|_{N_f=4}^{\text{NS}} &= 1 + 4.000000a + 24.392413a^2 - 737.300831a^3 \\
& - 23780.088207a^4 + O(a^5) \\
r^{\text{MOMggg}}(s) \Big|_{N_f=4}^{\text{NS}} &= 1 + 4.000000a - 26.908640a^2 - 1147.563910a^3 + O(a^4) \\
r^{\text{MOMh}}(s) \Big|_{N_f=4}^{\text{NS}} &= 1 + 4.000000a - 32.022911a^2 - 1111.886807a^3 + O(a^4) \\
r^{\text{MOMq}}(s) \Big|_{N_f=4}^{\text{NS}} &= 1 + 4.000000a - 24.692908a^2 - 769.140448a^3 + O(a^4) \\
r^{\text{mMOM}}(s) \Big|_{N_f=4}^{\text{NS}} &= 1 + 4.000000a - 14.163143a^2 - 1285.905875a^3 \\
& - 1366.112459a^4 + O(a^5)
\end{aligned} \tag{3.8}$$

$$\begin{aligned}
r^{\overline{\text{MS}}}(s) \Big|_{N_f=5}^{\text{NS}} &= 1 + 4.000000a + 22.547686a^2 - 817.092143a^3 \\
& - 20475.041592a^4 + O(a^5)
\end{aligned}$$

$$\begin{aligned}
r^{\text{MOMggg}}(s) \Big|_{N_f=5}^{\text{NS}} &= 1 + 4.000000a - 15.086140a^2 - 1102.107500a^3 + O(a^4) \\
r^{\text{MOMh}}(s) \Big|_{N_f=5}^{\text{NS}} &= 1 + 4.000000a - 29.423193a^2 - 1032.615604a^3 + O(a^4) \\
r^{\text{MOMq}}(s) \Big|_{N_f=5}^{\text{NS}} &= 1 + 4.000000a - 22.093189a^2 - 673.831312a^3 + O(a^4) \\
r^{\text{mMOM}}(s) \Big|_{N_f=5}^{\text{NS}} &= 1 + 4.000000a - 11.563425a^2 - 1196.136540a^3 \\
&\quad + 1629.497315a^4 + O(a^5)
\end{aligned} \tag{3.9}$$

and

$$\begin{aligned}
r^{\overline{\text{MS}}}(s) \Big|_{N_f=6}^{\text{NS}} &= 1 + 4.000000a + 20.702961a^2 - 897.546285a^3 \\
&\quad - 17413.037676a^4 + O(a^5) \\
r^{\text{MOMggg}}(s) \Big|_{N_f=6}^{\text{NS}} &= 1 + 4.000000a - 3.263641a^2 - 957.232297a^3 + O(a^4) \\
r^{\text{MOMh}}(s) \Big|_{N_f=6}^{\text{NS}} &= 1 + 4.000000a - 26.823475a^2 - 952.329471a^3 + O(a^4) \\
r^{\text{MOMq}}(s) \Big|_{N_f=6}^{\text{NS}} &= 1 + 4.000000a - 19.493471a^2 - 577.507245a^3 + O(a^4) \\
r^{\text{mMOM}}(s) \Big|_{N_f=6}^{\text{NS}} &= 1 + 4.000000a - 8.963706a^2 - 1105.352275a^3 \\
&\quad + 4256.595899a^4 + O(a^5) .
\end{aligned} \tag{3.10}$$

Interestingly the four loop term of the mMOM expression for each  $N_f$  value is an order of magnitude smaller than the  $\overline{\text{MS}}$  term, while the three loop term is consistently higher but not by the same amount. For the larger values of  $N_f$  the two loop term of the MOMq scheme is marginally smaller (in our conventions) than the  $\overline{\text{MS}}$  partner which would support the original observation of [5, 6]. This is also the case for the MOMggg scheme but not for MOMh. Both these schemes were not examined in [5, 6]. However, it should not be the case that the large variation in the corrections lead to significantly different interpretations of the  $R$ -ratio especially in the context of comparing with experimental data. Therefore we devote the next section to a more detailed analysis of these results.

## 4 Analysis.

For the first part of our analysis we note that we have reproduced the results of Table III of [6]. In that table the two loop correction to  $r^{\text{MOMq}}(s)$  was evaluated for each  $N_f$  at a particular value of the momentum and representative value of  $\Lambda^{\text{MOMq}}$ . It was compared to the same evaluation for the  $\overline{\text{MS}}$  scheme. The observation was that the higher order corrections appeared to improve the convergence with both schemes giving approximately the same values. In repeating this exercise we need to first recall the method used and within this append the necessary formalism to extend it to higher loop orders. First, we denote the running coupling constant at the  $L$ th loop order by  $a_L^{\mathcal{S}}(Q, \Lambda)$  and define each of the ones we require by

$$\begin{aligned}
a_2^{\mathcal{S}}(Q, \Lambda^{\mathcal{S}}) &= \frac{1}{b_0^{\mathcal{S}} L^{\mathcal{S}}} \left[ 1 - \frac{b_1^{\mathcal{S}} \ln(L^{\mathcal{S}})}{b_0^{\mathcal{S}2} L^{\mathcal{S}}} \right] \\
a_3^{\mathcal{S}}(Q, \Lambda^{\mathcal{S}}) &= \frac{1}{b_0^{\mathcal{S}} L^{\mathcal{S}}} \left[ 1 - \frac{b_1^{\mathcal{S}} \ln(L^{\mathcal{S}})}{b_0^{\mathcal{S}2} L^{\mathcal{S}}} + \left[ b_1^{\mathcal{S}2} \left[ \ln^2(L^{\mathcal{S}}) - \ln(L^{\mathcal{S}}) - 1 \right] + b_0^{\mathcal{S}} b_2^{\mathcal{S}} \right] \frac{1}{b_0^{\mathcal{S}4} L^{\mathcal{S}2}} \right]
\end{aligned}$$

$$\begin{aligned}
a_4^{\mathcal{S}}(Q, \Lambda^{\mathcal{S}}) = & \frac{1}{b_0^{\mathcal{S}} L^{\mathcal{S}}} \left[ 1 - \frac{b_1^{\mathcal{S}} \ln(L^{\mathcal{S}})}{b_0^{\mathcal{S}} L^{\mathcal{S}}} + \left[ b_1^{\mathcal{S}^2} \left[ \ln^2(L^{\mathcal{S}}) - \ln(L^{\mathcal{S}}) - 1 \right] + b_0^{\mathcal{S}} b_2^{\mathcal{S}} \right] \frac{1}{b_0^{\mathcal{S}^4} L^{\mathcal{S}^2}} \right. \\
& - \left[ b_1^{\mathcal{S}^3} \left[ \ln^3(L^{\mathcal{S}}) - \frac{5}{2} \ln^2(L^{\mathcal{S}}) - 2 \ln(L^{\mathcal{S}}) + \frac{1}{2} \right] + 3 b_0^{\mathcal{S}} b_1^{\mathcal{S}} b_2^{\mathcal{S}} \ln(L^{\mathcal{S}}) \right. \\
& \left. \left. - \frac{1}{2} b_0^{\mathcal{S}^2} b_3^{\mathcal{S}} \right] \frac{1}{b_0^{\mathcal{S}^6} L^{\mathcal{S}^3}} \right]
\end{aligned} \tag{4.1}$$

for each scheme  $\mathcal{S}$  where

$$L^{\mathcal{S}} = \ln \left( \frac{Q^2}{\Lambda^{\mathcal{S}^2}} \right). \tag{4.2}$$

We note that there are different choices for the higher order expressions but we have chosen to take the definitions recorded in the review in [35]. Next if we define the perturbative coefficients of  $r^{\mathcal{S}}(s)$  via

$$r^{\mathcal{S}}(s) = \sum_{n=0}^{\infty} r_n^{\mathcal{S}}(s) a^{\mathcal{S}n} \tag{4.3}$$

where  $r_0^{\mathcal{S}} = 1$  for all schemes then we can define the partial sums of the series by

$$a_{pq}^{\mathcal{S}} \left( \frac{Q^2}{\Lambda^{\mathcal{S}^2}} \right) = \sum_{n=1}^p r_n^{\mathcal{S}}(s) \left( a_q^{\mathcal{S}}(Q, \Lambda^{\mathcal{S}}) \right)^n. \tag{4.4}$$

We note that the series starts from the  $O(a)$  term and hence one has in effect defined an effective coupling constant whose root is in the  $R$ -ratio. Indeed as a side comment we note that this is a starting point for the method of effective charges discussed in [36, 37, 38, 39]. In [7] the three loop  $\beta$ -function for this effective charge was constructed based on the formalism given in [38]. We have repeated this exercise as part of the check on our partial sum construction here in each of the MOM schemes of interest and found that they are all formally equivalent. This is as it should be since the  $\beta$ -function of this effective charge method is a renormalization group invariant.

$p$	$q$	$\overline{\text{MS}}$	MOMggg	MOMh	MOMq	mMOM
1	1	0.0707	0.0848	0.0918	0.0881	0.0833
1	2	0.0581	0.0683	0.0733	0.0707	0.0672
1	3	0.0592	0.0699	0.0753	0.0681	0.0695
1	4	0.0571				0.0698
2	2	0.0629	0.0639	0.0635	0.0638	0.0640
2	3	0.0641	0.0653	0.0649	0.0617	0.0661
2	4	0.0643				0.0663
3	3	0.0615	0.0594	0.0580	0.0584	0.0598
3	4	0.0616				0.0599
4	4	0.0606				0.0601

Table 2. Values of  $a_{pq}^{\mathcal{S}} \left( \frac{Q^2}{\Lambda^{\mathcal{S}^2}} \right)$  for  $N_f = 5$  with  $\Lambda^{\overline{\text{MS}}} = 500\text{MeV}$  and  $Q = 20\text{GeV}$ .

Returning to the comparison with Table III of [6] in the present notation the results which were presented in [6] were  $a_{12}^{\mathcal{S}}$  and  $a_{22}^{\mathcal{S}}$  for  $\overline{\text{MS}}$  and MOMq with  $Q = 3, 5, 20$  and  $40\text{GeV}$  respectively for  $N_f = 3, 4, 5$  and  $6$ . The choices for the values of  $\Lambda$  were  $\Lambda^{\overline{\text{MS}}} = 500\text{MeV}$  and  $\Lambda^{\text{MOMq}} = 850\text{MeV}$ . From the formalism given here with these specific values it is straightforward to recover Table III of [6]. However, we have extended it for each of the MOM schemes as well

as for the  $\overline{\text{MS}}$  scheme. The results for  $N_f = 5$  are given in Table 2 with Table 3 corresponding to the  $N_f = 6$  case. Several general comments are in order. First, for MOMggg, MOMh and MOMq the absent entries are due to the fact that the four loop  $\beta$ -functions for these schemes are not known. Next, in each Table we have used  $\Lambda^{\overline{\text{MS}}} = 500\text{MeV}$  for each of the values of  $N_f$ .

$p$	$q$	$\overline{\text{MS}}$	MOMggg	MOMh	MOMq	mMOM
1	1	0.0652	0.0723	0.0809	0.0780	0.0742
1	2	0.0566	0.0622	0.0690	0.0667	0.0637
1	3	0.0569	0.0617	0.0688	0.0634	0.0641
1	4	0.0571				0.0645
2	2	0.0608	0.0614	0.0610	0.0613	0.0615
2	3	0.0611	0.0609	0.0609	0.0585	0.0618
2	4	0.0613				0.0621
3	3	0.0585	0.0574	0.0560	0.0562	0.0572
3	4	0.0587				0.0575
4	4	0.0580				0.0580

Table 3. Values of  $a_{pq}^S \left( \frac{Q^2}{\Lambda^2} \right)$  for  $N_f = 6$  with  $\Lambda^{\overline{\text{MS}}} = 500\text{MeV}$  and  $Q = 40\text{GeV}$ .

This is merely to gain a general appreciation of the effect of including higher order corrections but a different choice could be made. Rather than take  $\Lambda^{\text{MOMq}}$  to be 850MeV we use the values of the  $\Lambda$  parameter ratios for the Landau gauge given in Table 1. The small variation in the ratio for MOMq appears to be the justification behind the choice of 850MeV used in [6] for all values of  $N_f$  considered there. However, we have chosen to apply the more precise ratios here mainly because the variation over the range in  $N_f$  is more significant for several of the other schemes. Therefore, the values given in Tables 2 and 3 which are to be compared to those in [6] will not be precisely the same for this reason. Though we emphasise that taking the same values of the momentum and parameters used in [6] we do find exact agreement. We have not provided tables for  $N_f = 3$  and 4 because the values of  $Q$  used in [6] are too low. At three loops for these values of  $Q$  the contributions from the logarithm are large and affect the analysis.

Examining the entries in Tables 2 and 3 perhaps a reasonable guide to the rate of convergence can be seen from looking at the values for  $a_{LL}^S$  at the  $L$ th loop. Though in this discussion we exclude  $L = 1$  as it has no true contact with loop corrections. For  $\overline{\text{MS}}$  and mMOM there are three such terms and for both  $N_f = 5$  and 6 it appears that not only both converge but they seem to be converging to the same value. In most cases the convergence is not monotonic decreasing unlike for  $N_f = 5$  for the  $\overline{\text{MS}}$  scheme. For the other three schemes there are only two values to comment on and while each appear to be roughly the same value for  $L = 3$  a conclusion cannot really be drawn as to the final value. Although they are not dissimilar to the corresponding number for the mMOM scheme. More instructive in understanding the situation is to examine plots of these partial sums for each of the schemes. In Figures 1 and 2 we have plotted  $a_{LL}^S(x)$  for  $L = 3$  and 4 respectively for each of the four values of  $N_f$  where we use the dimensionless variable  $x$  as shorthand for  $x = s/\Lambda$ . Although we only have two schemes to compare in Figure 2. Unlike the data in Tables 2 and 3, for the plots we provide we do not fix the value of  $\Lambda^{\overline{\text{MS}}}$  but use it as the reference  $\Lambda$  to which the parameter in the other schemes are related to it by the ratios in Table 1. We have not provided the graphs for the two loop case as the lines for all the schemes lie on top of each other. This is because at this order the scheme dependence cancels out from the  $\Lambda$  parameter relation and the coupling constant map as well as the fact that in the Landau gauge the one and two loop coefficients of each  $\beta$ -function are the same. Only at

three loops does the scheme dependence become evident which is due in the main to the scheme differences in  $b_3^S$ . Indeed it is for this reason that scheme issues could not be examined in the  $R$ -ratio until the three loop MOM QCD  $\beta$ -functions were known, [20]. However for larger values of  $Q$  the variation in values between each scheme diminishes which is not unexpected. At three

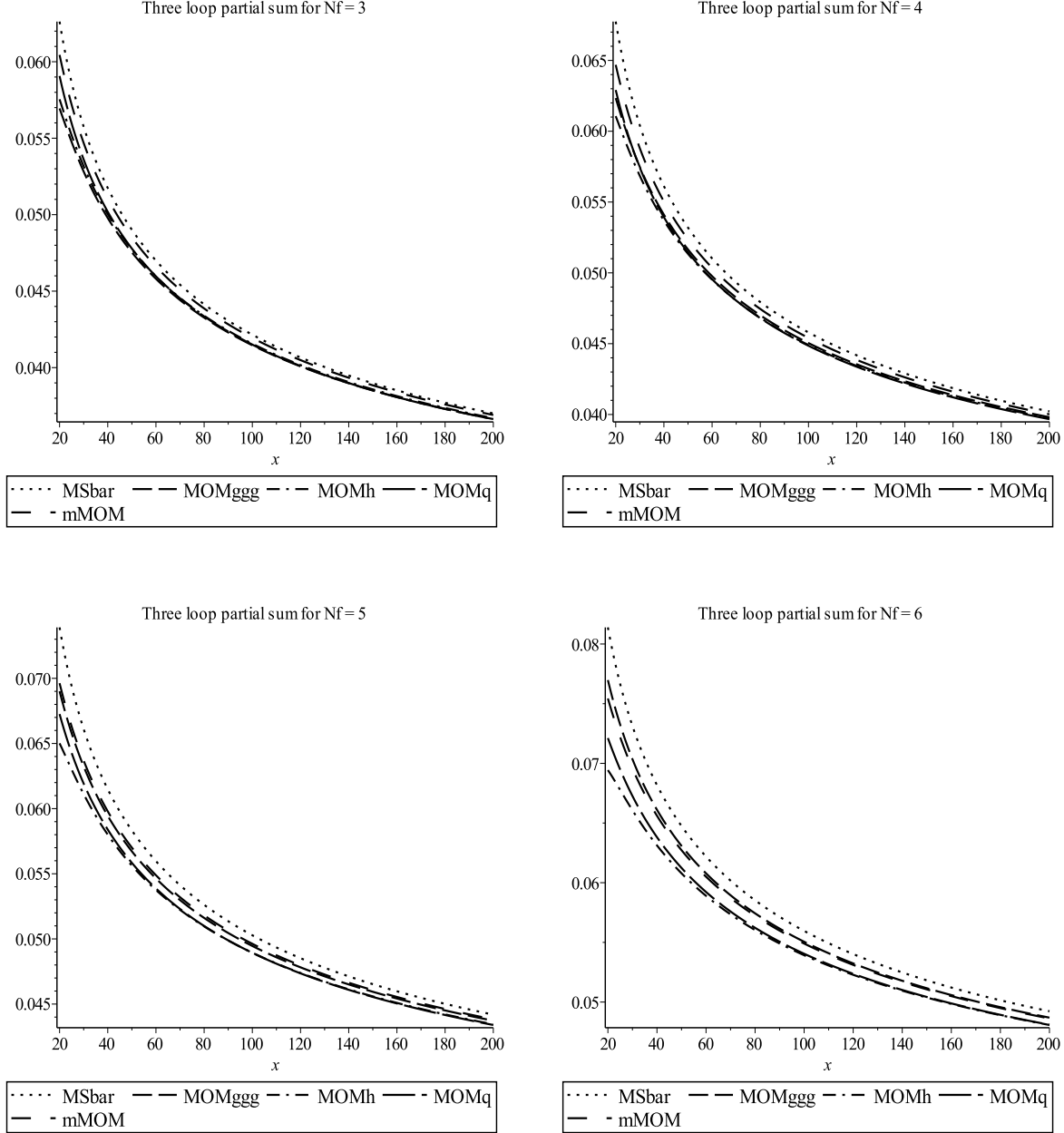


Figure 1: Comparison of  $a_{33}^S(x)$  for the various schemes for  $N_f = 3, 4, 5$  and  $6$ .

loops the variation in values is not huge for  $x = 20$  except for  $N_f = 6$ . With these plots one can examine the values in Tables 2 and 3. Recalling that for these if we have  $\Lambda^{\overline{\text{MS}}} = 500\text{MeV}$  then at  $x = 80$  in the  $N_f = 5$  and  $6$  plots of Figure 1 we can see that the MOMggg and mMOM scheme values are on a par with each other. Additionally the MOMh and MOMq lines are virtually the same with the  $\overline{\text{MS}}$  line appearing to be at odds with both. Although at four loops we have only two schemes to compare with there is very little to distinguish the curves for all values of  $N_f$ . As discussed earlier this may be due to these schemes being of a similar nature.

While this comparison between schemes is instructive in observing over what ranges the schemes give similar values for the partial sums, it is also useful to compare the convergence within each scheme for  $a_{LL}^S(x)$ . We have provided these plots in Figures 3, 4, 5, 6 and 7 for the  $\overline{\text{MS}}$ , MOMggg, MOMh, MOMq and mMOM schemes respectively for  $L = 2, 3$  and 4.

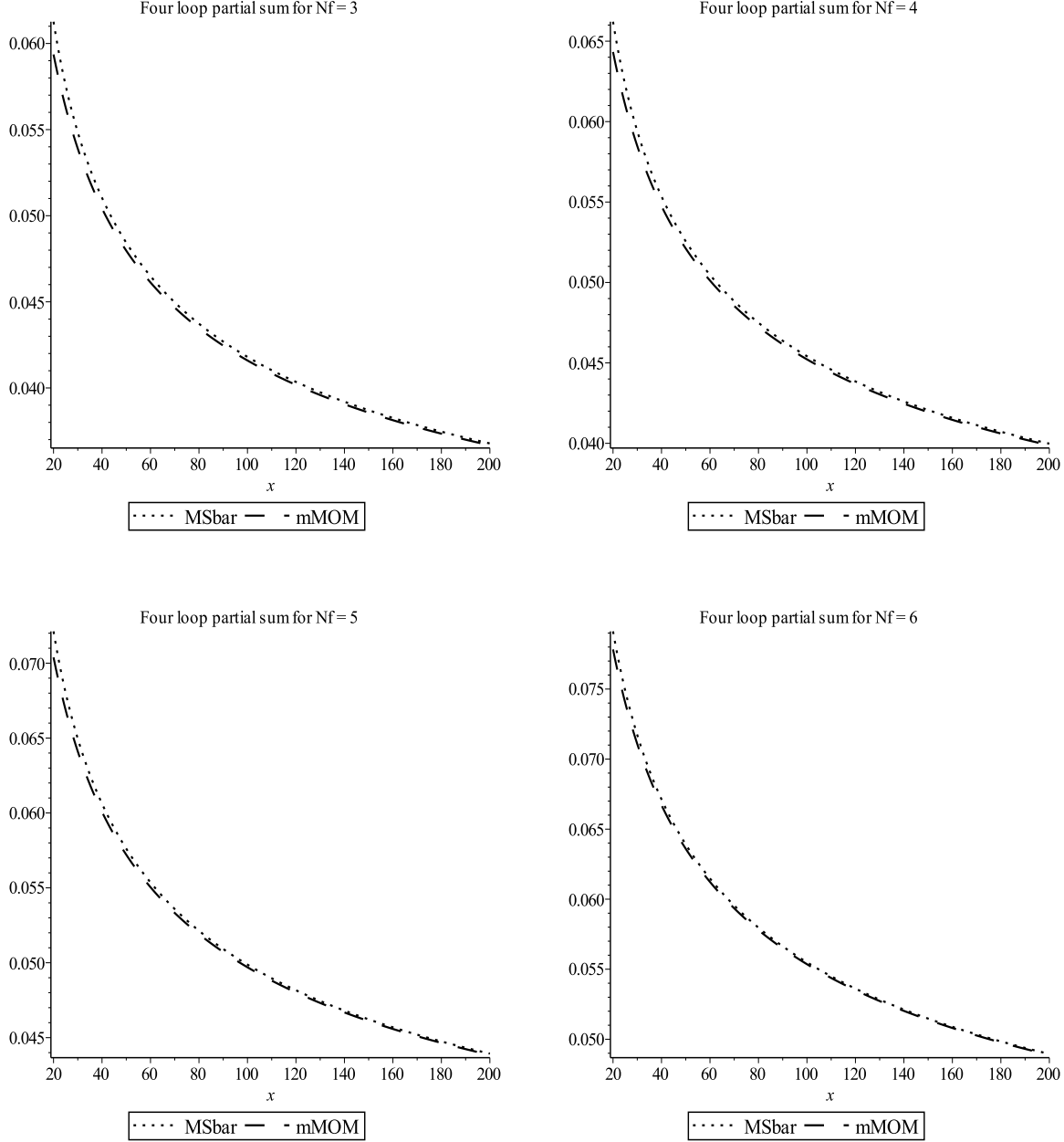


Figure 2: Comparison of  $a_{44}^S(x)$  for  $\overline{\text{MS}}$  and mMOM for  $N_f = 3, 4, 5$  and 6.

Overall the partial sums decrease in value as  $L$  increases, with the largest reduction being for larger values of  $N_f$ . For the two cases where four loop information is available the four loop plots are not significantly different from the three loop ones. This would be consistent with the observation that an increase in loop order may not improve precision by very much. However, the situation with the other three schemes is not conclusive. Each share the same property that there is a relatively large drop in the value from  $L = 2$  to 3. In light of a similar observation for the  $\overline{\text{MS}}$  and mMOM cases this would suggest that a determination of

the four loop  $\beta$ -function would appear necessary in order to see whether that correction was significantly different from the three loop one. Once that was resolved the main issue would be if each of the schemes gave a similar precision. The curves in Figure 2 would be encouraging in this respect. However, this has to be tempered with the fact that both the  $\overline{\text{MS}}$  and mMOM

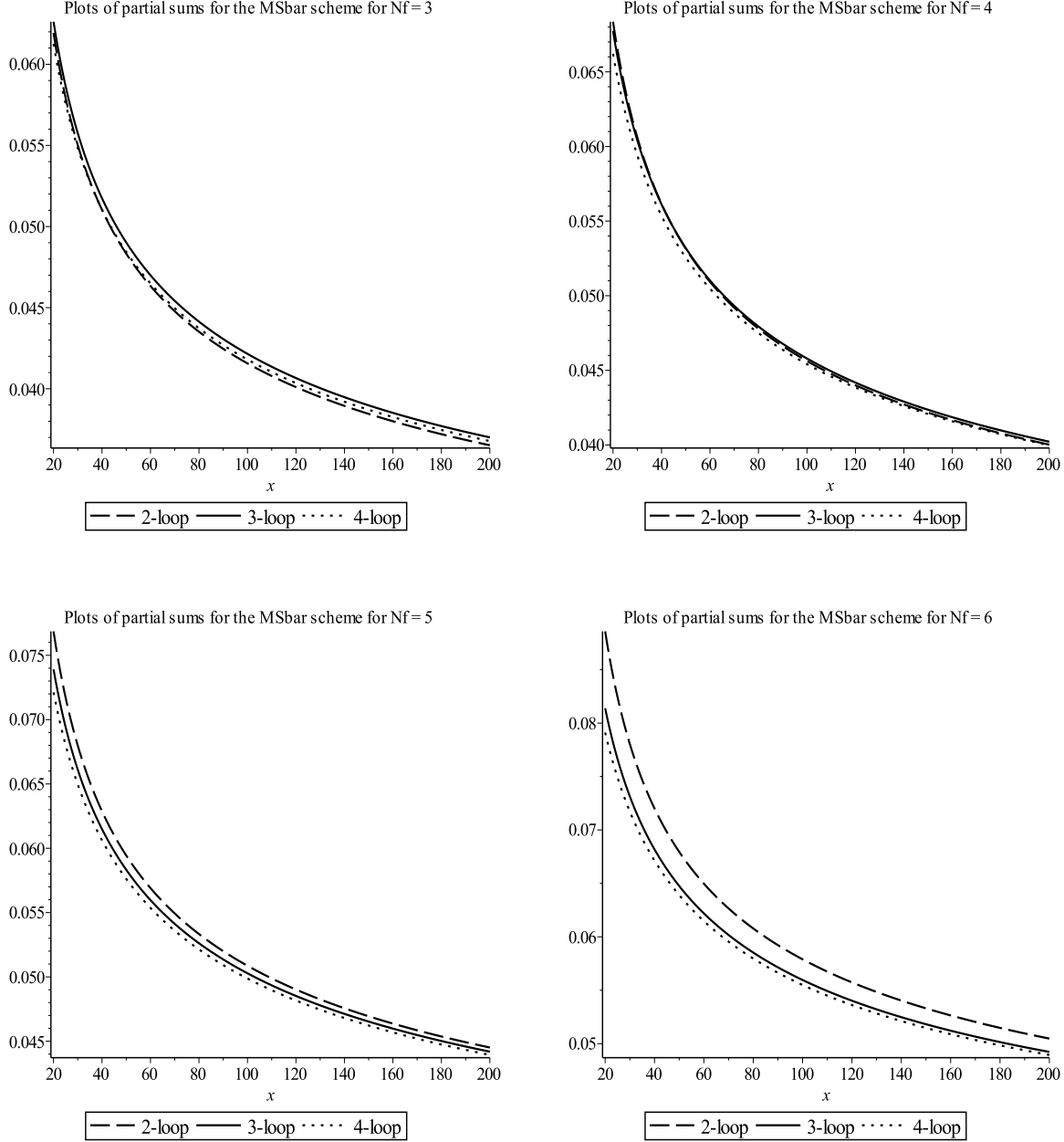


Figure 3: Plots of  $a_{LL}^{\overline{\text{MS}}}(x)$  for  $L = 2, 3$  and  $4$ .

schemes have a similar aspect in their definition. In some sense they are related to an external momentum configuration of the vertex function where the subtraction is defined at a point where one external leg is nullified. This is evident for the mMOM scheme. For the  $\overline{\text{MS}}$  scheme it is less apparent. To determine the renormalization constants for the coupling constant in QCD in  $\overline{\text{MS}}$  there are several computational approaches. For reasons of calculational ease for each of the three 3-point vertices in the QCD Lagrangian one can set the external momentum of a specific leg to zero. This reduces all the Feynman graphs in effect to 2-point ones and so the

extraction of the poles in the regularizing parameter are no more difficult than in computing the poles for the wave function renormalization. Moreover, this nullification procedure, known as infrared rearrangement [18, 19], does not introduce any infrared problems. A nullified external

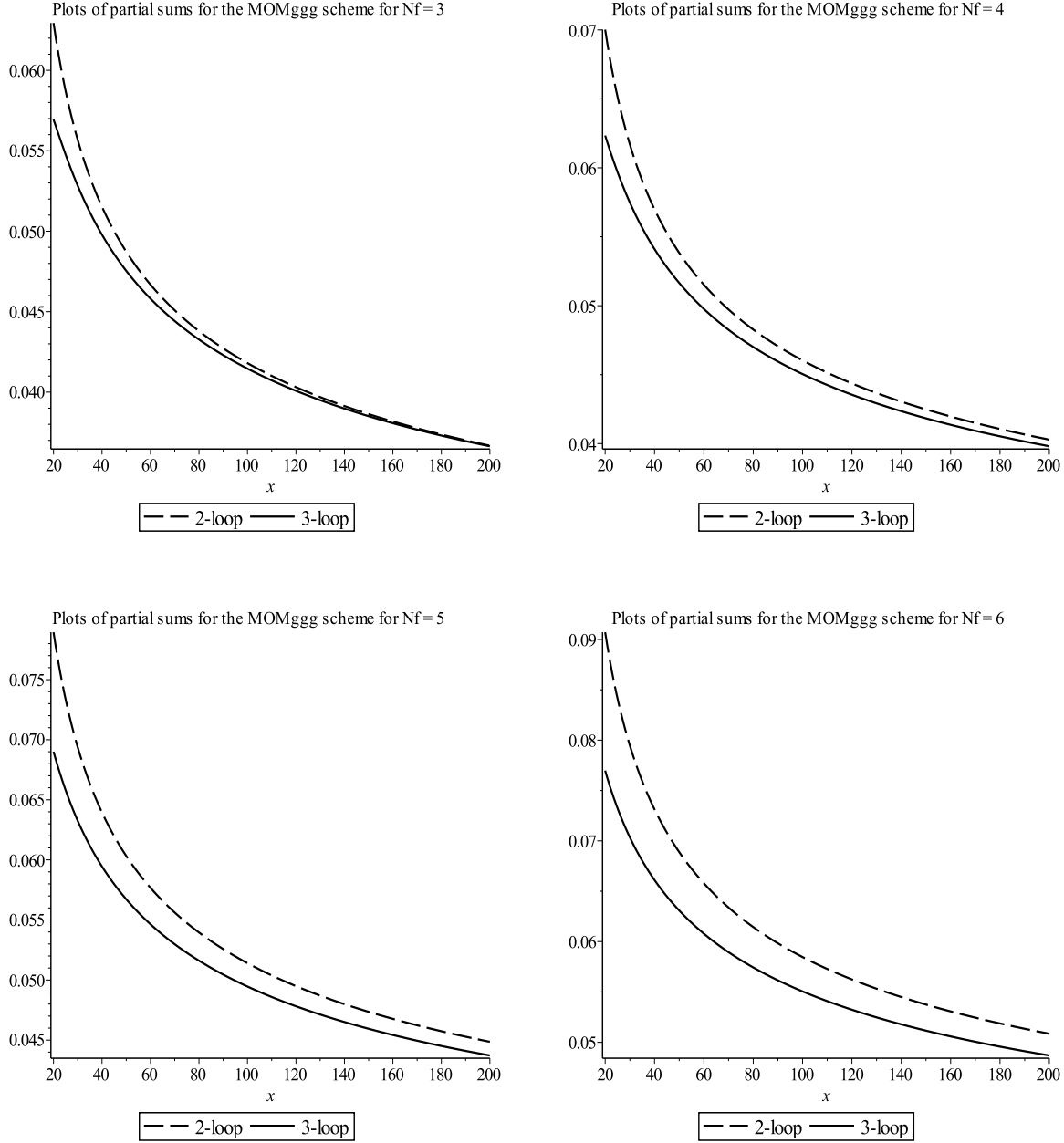


Figure 4: Plots of  $a_{LL}^{\text{MOMggg}}(x)$  for  $L = 2$  and 3.

momentum means that either the quark or gluon is on-shell. While this is an efficient method to determine the  $\overline{\text{MS}}$  coupling constant renormalization which has allowed for the construction of the  $\beta$ -function at very high loop order, [30], one does not have to apply a nullification. Instead it is possible to extract the  $\overline{\text{MS}}$  coupling constant renormalization constant at more general momentum configurations. Indeed in the original MOM approach of [16, 17] the  $\overline{\text{MS}}$  renormalization was carried out at the fully symmetric point at one loop. Moreover, in [20] this was used as a computational check on the extension to two loops as well as for the general off-shell case, [40]. However, in the context of  $\overline{\text{MS}}$  and mMOM being similar this independence of the

definition of the  $\overline{\text{MS}}$  scheme to the subtraction point is what makes it akin to the mMOM scheme where a nullification is inherent in the construction. The  $\overline{\text{MS}}$  scheme can be defined at a nullified point. In the context of perturbative quantum field theory this is somewhat unnatural. (We

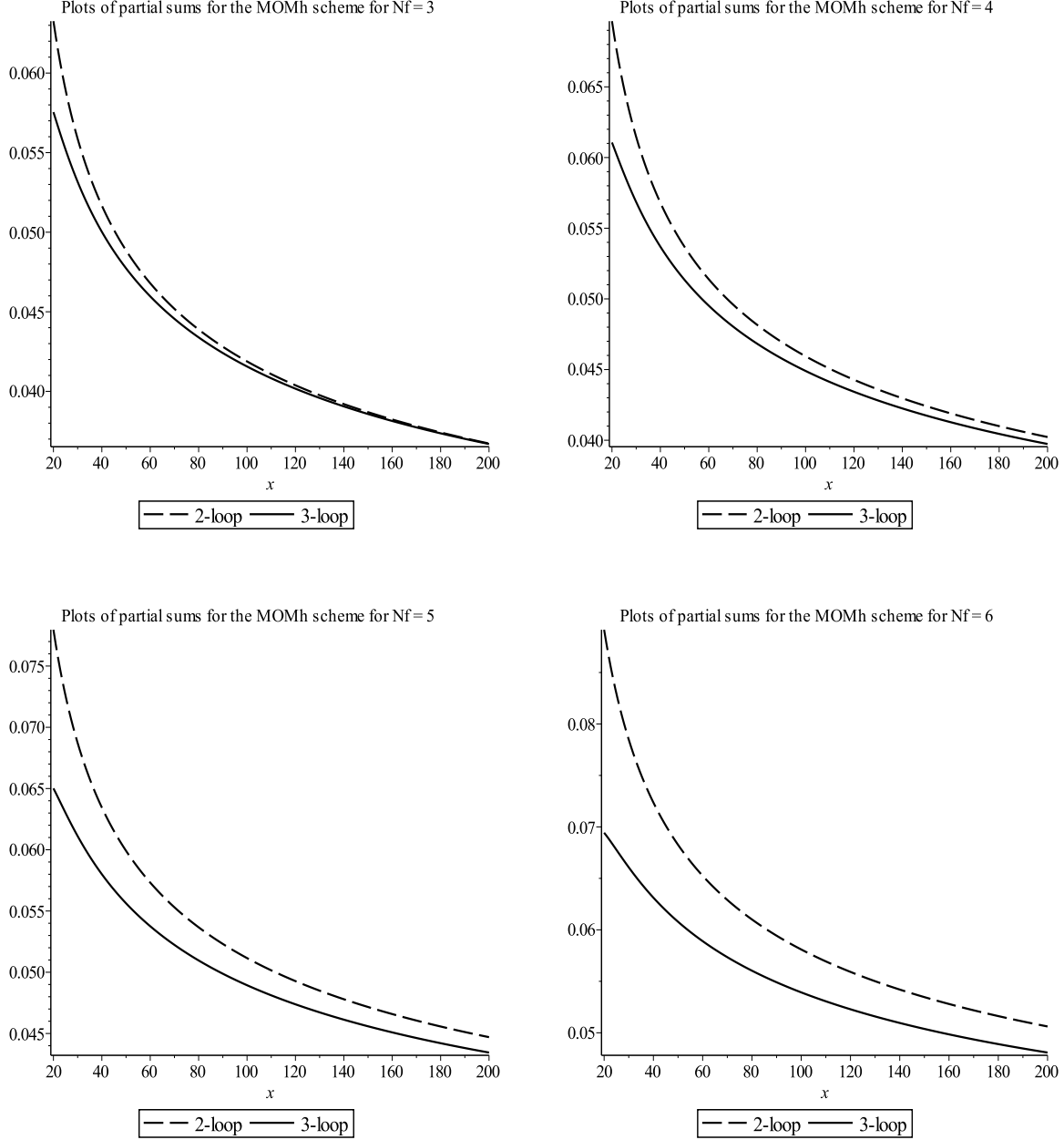


Figure 5: Plots of  $a_{LL}^{\text{MOMh}}(x)$  for  $L = 2$  and 3.

recall that we are using chiral quarks here.) Therefore, the coupling constant renormalization is being examined at a point where such entities do not exist as fundamental quanta. In other words the definition of the  $\overline{\text{MS}}$  renormalization constant carries with it no connection of where it is defined. By contrast the MOM schemes of [16, 17] do since they incorporate information of the symmetric subtraction point through the inclusion of a finite part in the coupling constant renormalization constant. Moreover, as no external legs have been nullified there is no issue with the interpretation of the fields corresponding to fundamental particles. In another sense a momentum subtraction scheme would appear to be more natural for a physical coupling as the

finite part could be regarded as a measure of the associated radiation. Therefore, in order to resolve some of these observations it would again seem necessary to extend the MOM  $\beta$ -functions of [16, 17] to four loops.

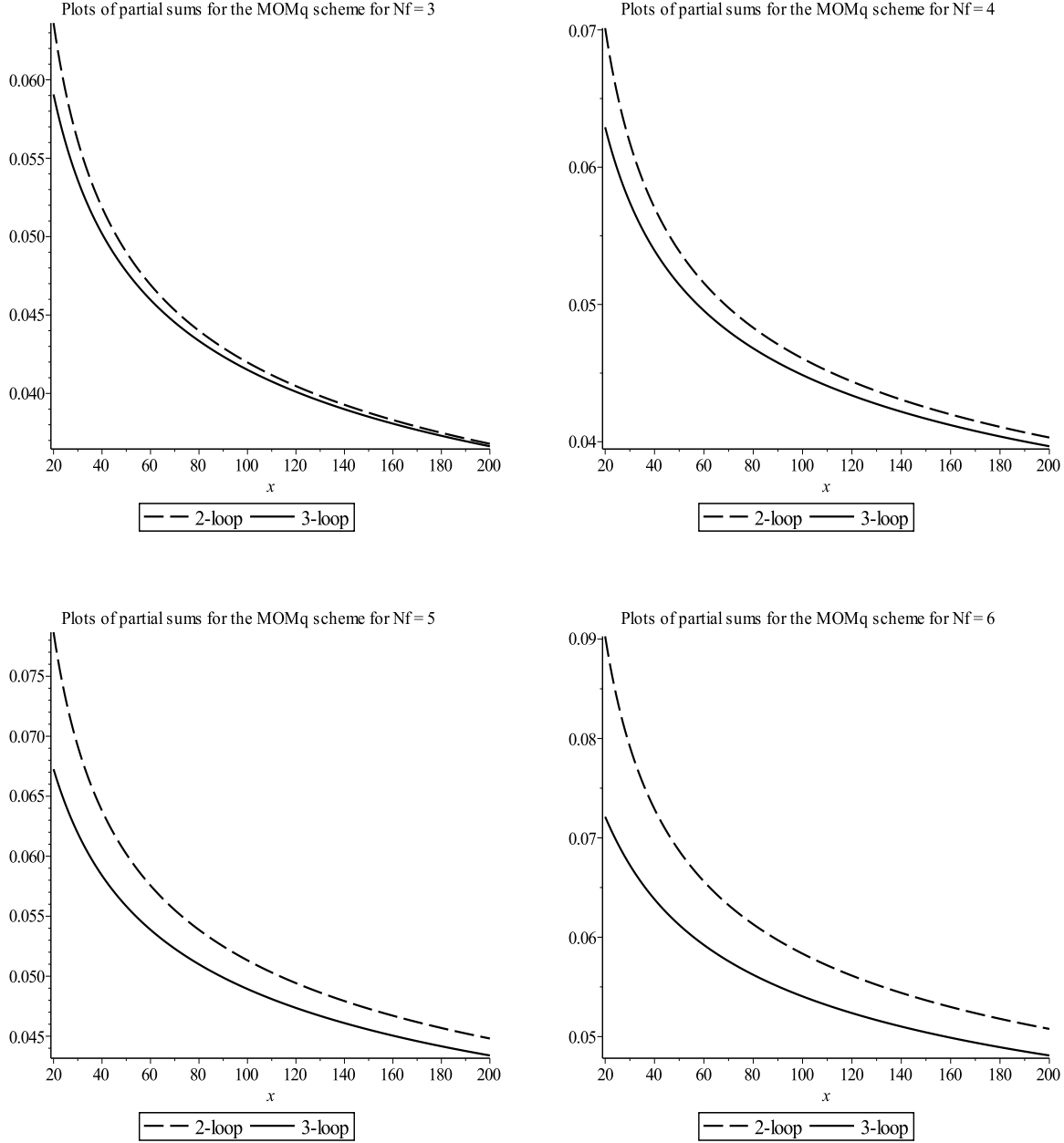


Figure 6: Plots of  $a_{LL}^{\text{MOMq}}(x)$  for  $L = 2$  and 3.

While we have focused exclusively to this point on the Landau gauge for the MOM schemes for the reasons we stated earlier, it is worth considering the dependence on the gauge parameter as an exercise. For this we have analysed the MOMq scheme for various values of  $\alpha$  and the same values of  $N_f$  as before. For this investigation the same formalism is used where now the  $\alpha$  dependent coefficients of the three loop MOMq  $\beta$ -function must be included and are available from [16, 17, 20]. Equally the  $\alpha$  dependent MOMq three loop  $R$ -ratio is constructed from the three loop coupling constant map. As the  $\overline{\text{MS}}$   $R$ -ratio is gauge parameter independent we do not have to include the mapping of the gauge parameter variable from one scheme to another.

The gauge parameter dependence arises solely from the coupling constant map. In addition we

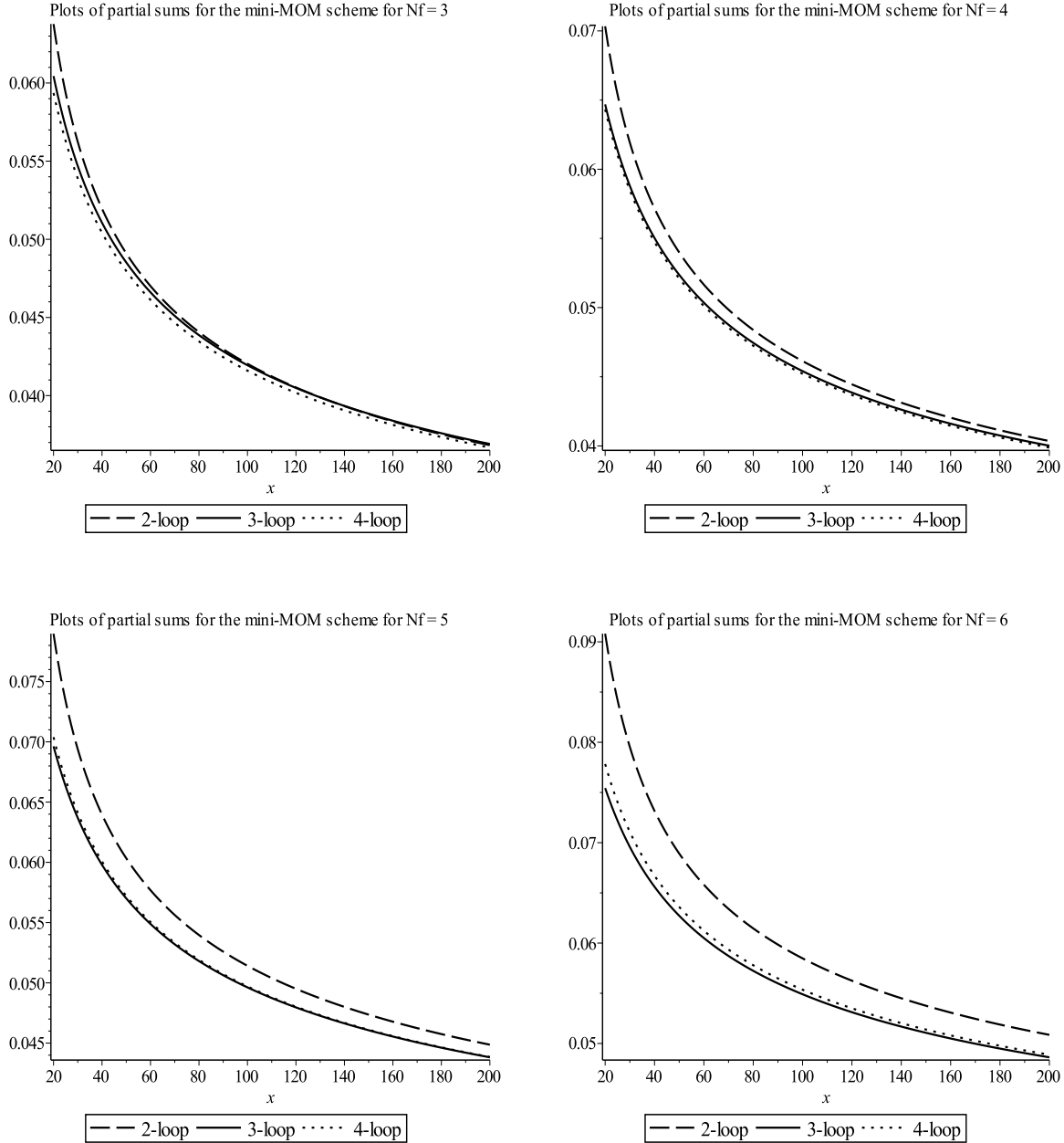


Figure 7: Plots of  $a_{LL}^{\text{mMOM}}(x)$  for  $L = 2, 3$  and  $4$ .

also have to use the  $\alpha$  dependent  $\Lambda$  parameter ratios which are straightforward to extract from the formulæ given in [16, 17]. In order to assist with the comparison of earlier plots we give the same partial sums as before for two loops in Figure 8 and three loops in Figure 9. In both the quantity  $\mathbf{a1}$  corresponds to the canonical gauge parameter  $\alpha$  with  $\alpha = 0$  corresponding to the earlier Landau gauge results. The plots for that gauge are repeated in both figures as the benchmark to compare with. We have not provided comparison plots between loops since it is the variation in the behaviour for various  $\alpha$  which is of interest. The largest value of  $\alpha$  we have taken is 10 as anything beyond this has a significantly small  $\Lambda$  ratio. From Figure 8 for each value of  $N_f$   $a_{22}^{\text{MOMq}}(x)$  gets progressively smaller as  $\alpha$  increases. The main point is that as  $\alpha$  increases the partial sum diverges from not only the Landau gauge MOMq value but also the

$\overline{\text{MS}}$  value. This is more evident in the plots of Figure 9 where the non-zero  $\alpha$  lines cover a broad range especially for relatively small values of  $x$ . If one recalls the earlier comparisons of MOMq for the Landau gauge with the other schemes while there is clearly not precise agreement there is not a broad range suggesting convergence. Such a convergence is difficult to perceive from using various fixed values for  $\alpha$  as can be seen in Figures 8 and 9 which suggests the Landau gauge is the appropriate choice for a MOM scheme analysis.

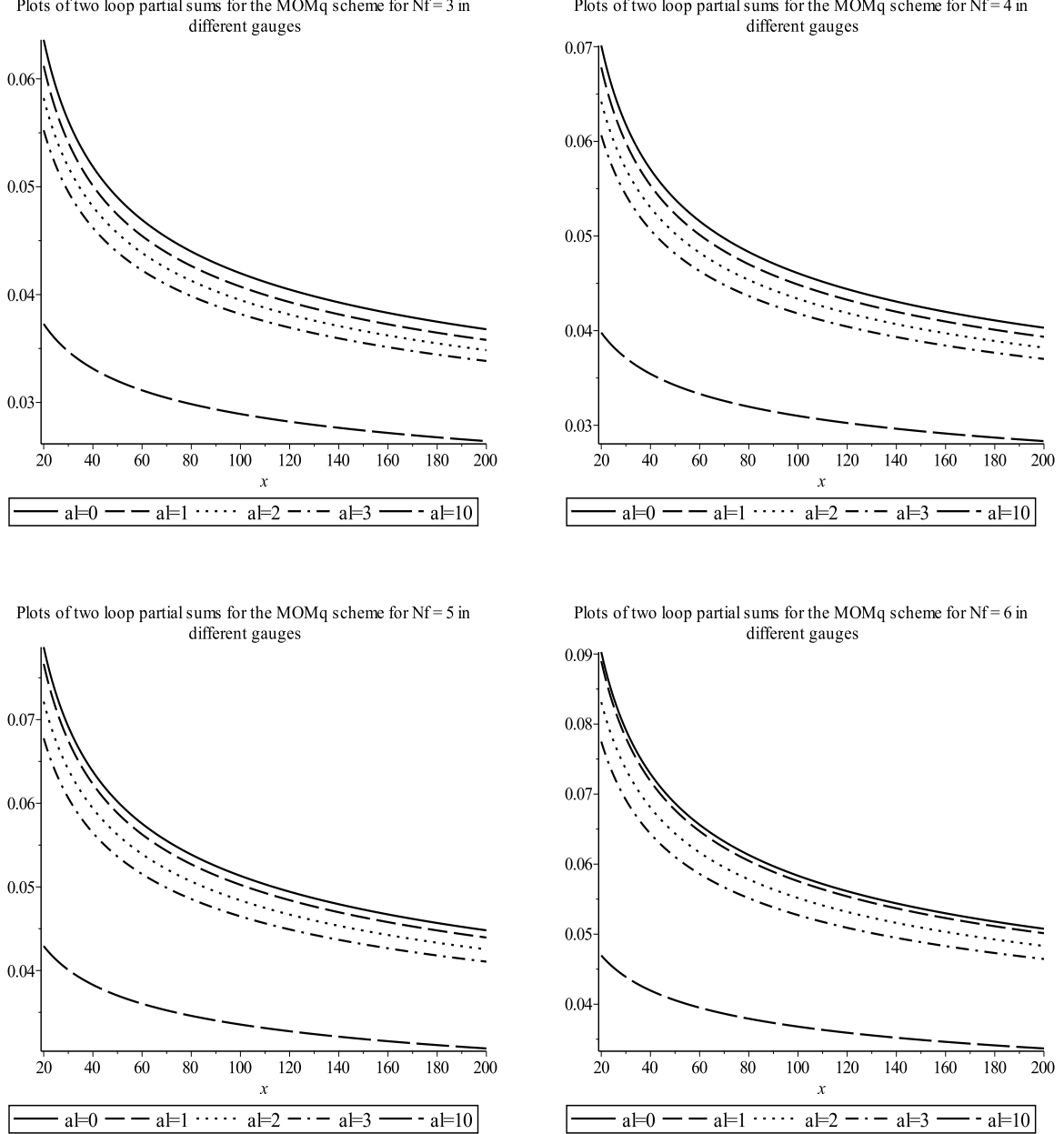


Figure 8: Plots of  $a_{22}^{\text{MOMq}}(x)$  for various gauges.

## 5 Discussion.

We have completed an analysis of the  $R$ -ratio in various MOM renormalization schemes. One motivation was to extend the early computations of [5, 6] to the next loop order since the two loop mappings of the coupling constants between the  $\overline{\text{MS}}$  and MOM schemes of [16, 17] as well as the three loop MOMggg, MOMh and MOMq  $\beta$ -functions are now available, [20]. Another aim was to examine whether the observation of [5, 6] that the MOMq scheme led to an improved or better convergent series for a physical quantity held at next order. In general terms it

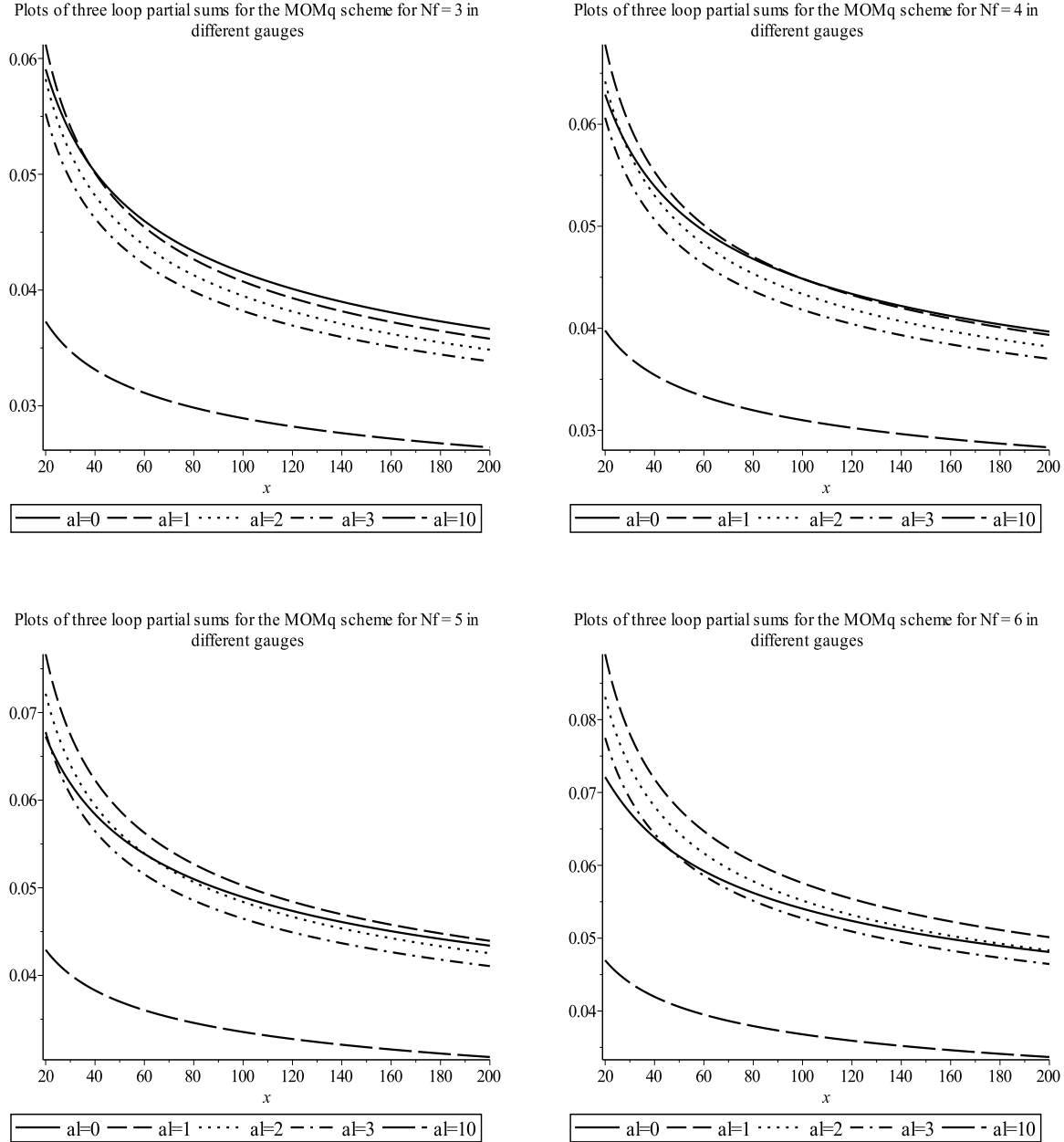


Figure 9: Plots of  $a_{33}^{\text{MOMq}}(x)$  for various gauges.

does not appear to be the case. By this we mean that from the numerical values, (3.7)-(3.10), while the magnitude of some of the MOMi schemes  $L$ -loop coefficients may be smaller than their  $\overline{\text{MS}}$  counterpart, at the next order this position may be reversed. Indeed the sign of the

corresponding terms is not preserved between schemes. This is not unexpected as there is no general reason why this should be. However, it could give the impression that convergence of the series in one scheme is better than another. This is not the case as can be seen from the various plots provided here. Once the running coupling constant as a function of the  $\Lambda$  parameter associated with that scheme is included, as well as its relation to  $\Lambda^{\overline{\text{MS}}}$  as the reference scale, then the partial sums plotted against the momentum scale are generally comparable across schemes. Overall there is little difference between the results for large momentum as expected. It is at lower values where there are differences. However, the actual discrepancy is not significant. Moreover, within schemes there appears to be little difference for  $\overline{\text{MS}}$  and mMOM between the three and four loop partial sums. At present the four loop MOMggg, MOMh and MOMq schemes can not be examined at this level but it would be worth pursuing. This is because of the fact that the MOM schemes are in some sense more physical in that they are defined at a subtraction point which is completely symmetric and the momentum configuration there is non-exceptional. Indeed this would resolve whether there is actually a difference between the  $\overline{\text{MS}}$  and MOMq results as suggested in the  $N_f = 6$  plot of Figure 1. By contrast the  $\overline{\text{MS}}$  scheme is essentially independent of the momentum subtraction point and to all intents and purposes does not carry any information about the structure of the vertex which is encoded in the finite parts of the coupling constant renormalization in the MOMggg, MOMh and MOMq schemes. In this context and from the plots mMOM is more akin to  $\overline{\text{MS}}$  partly due to the fact that it is defined at a subtraction point which is exceptional. In carrying information about the vertex structure in the associated renormalization constant that information differs from the MOMggg, MOMh and MOMq schemes because mMOM has an off-shell leg. Within certain plots where the schemes were compared there is a suggestion that the exceptional based schemes are slightly different from the other three schemes. However, it is not possible to draw a definite conclusion on this before the full four loop MOMggg, MOMh and MOMq scheme  $\beta$ -functions are known. Though one conclusion which seems to be assured is that the Landau gauge is the gauge which one should only consider when applying the MOMi schemes. While we have focused on the  $R$ -ratio here it would be interesting to examine high loop evaluations of other physical quantities in order to see if one can make similar or general observations about the MOM schemes of [16, 17].

**Acknowledgements.** The author thanks J.M. Bell, D.J. Broadhurst, M. Gorbahn, D. Kreimer and E. Panzer for valuable discussions as well as the organisers of the Summer School on Structures in Local Quantum Field Theory held at Les Houches, France where the work was initiated. The Mathematical Physics Group at Humboldt University, Berlin, where part of the work was carried out, is also thanked for its hospitality.

## References.

- [1] T. Appelquist & H. Georgi, Phys. Rev. **D8** (1973), 2000.
- [2] A. Zee, Phys. Rev. **D8** (1973), 4038.
- [3] K.G. Chetyrkin, A.L. Kataev & F.V. Tkachov, Phys. Lett. **B85** (1979), 277.
- [4] M. Dine & J. Sapiirstein, Phys. Rev. Lett. **43** (1979), 668.
- [5] W. Celmaster & R.J. Gonsalves, Phys. Rev. Lett. **44** (1980), 560.
- [6] W. Celmaster & R.J. Gonsalves, Phys. Rev. **D21** (1980), 3112.

- [7] S.G. Gorishnii, A.L. Kataev & S.A. Larin, Phys. Lett. **B212** (1988), 238.
- [8] S.G. Gorishnii, A.L. Kataev & S.A. Larin, Phys. Lett. **B259** (1991), 144.
- [9] L.R. Surguladze & M.A. Samuel, Phys. Rev. Lett. **66** (1991), 560.
- [10] P.A. Baikov, K.G. Chetyrkin & J.H. Kühn, Phys. Rev. Lett. **104** (2010), 132004.
- [11] P.A. Baikov, K.G. Chetyrkin, J.H. Kühn & J. Rittinger, Phys. Rev. Lett. **108** (2012), 222003.
- [12] P.A. Baikov, K.G. Chetyrkin & J.H. Kühn, Phys. Lett. **B714** (2012), 62.
- [13] K.G. Chetyrkin, R.V. Harlander & J.H. Kühn, Nucl. Phys. **B586** (2000), 56; Nucl. Phys. **B634** (2002), 413(E).
- [14] K.G. Chetyrkin, B.A. Kniehl & M. Steinhauser, Nucl. Phys. **B814** (2009), 231.
- [15] W.A. Bardeen, A.J. Buras, D.W. Duke & T. Muta, Phys. Rev. **D18** (1978), 3998.
- [16] W. Celmaster & R.J. Gonsalves, Phys. Rev. Lett. **42** (1979), 1435.
- [17] W. Celmaster & R.J. Gonsalves, Phys. Rev. **D20** (1979), 1420.
- [18] A.A. Vladimirov, Theor. Math. Phys. **43** (1980), 417.
- [19] K.G. Chetyrkin, A.L. Kataev & F.V. Tkachov, Nucl. Phys. **B174** (1980), 345.
- [20] J.A. Gracey, Phys. Rev. **D84** (2011), 085011.
- [21] L. von Smekal, K. Maltman & A. Sternbeck, Phys. Lett. **B681** (2009), 336.
- [22] K.G. Chetyrkin & A. Rétey, hep-ph/0007088.
- [23] J.A. Gracey, J. Phys. **A46** (2013), 225403.
- [24] J.C. Taylor, Nucl. Phys. **B33** (1971), 436.
- [25] G. 't Hooft, Nucl. Phys. **B61** (1973), 455.
- [26] D.J. Gross & F.J. Wilczek, Phys. Rev. Lett. **30** (1973), 1343.
- [27] H.D. Politzer, Phys. Rev. Lett. **30** (1973), 1346.
- [28] W.E. Caswell, Phys. Rev. Lett. **33** (1974), 244.
- [29] D.R.T. Jones, Nucl. Phys. **B75** (1974), 531.
- [30] O.V. Tarasov, A.A. Vladimirov & A.Yu. Zharkov, Phys. Lett. **B93** (1980), 429.
- [31] T. van Ritbergen, J.A.M. Vermaseren & S.A. Larin, Phys. Lett. **B400** (1997), 379.
- [32] M. Czakon, Nucl. Phys. **B710** (2005), 485.
- [33] L.G. Almeida & C. Sturm, Phys. Rev. **D82** (2010), 054017.
- [34] M. Gorbahn & S. Jäger, Phys. Rev. **D82** (2010), 114001.
- [35] J. Beringer et al. (Particle Data Group), Phys. Rev. **D86** (2012), 010001.

- [36] G. Grunberg, Phys. Lett. **B95** (1980), 70; Phys. Lett. **B110** (1982), 501(E).
- [37] P.M. Stevenson, Phys. Lett. **B100** (1981), 61.
- [38] P.M. Stevenson, Phys. Rev. **D23** (1981), 2916.
- [39] G. Grunberg, Phys. Rev. **D29** (1984), 2315.
- [40] J.A. Gracey, Phys. Rev. **D90** (2014), 025014.